4-6-2017

Improving Estimates of Phytoplankton Populations in the Chesapeake Bay Using Hyperspectral Radiometers

Max Spehlmann
Lake Forest College, spehlmannm@lakeforest.edu

Improving Estimates of Phytoplankton Populations in the Chesapeake Bay Using Hyperspectral Radiometers

Abstract
In coastal and estuarine waters, high turbidity and land interference severely diminish the utility of satellite data. This study tested the accuracy of hyperspectral inversion algorithms to better resolve chlorophyll a estimates in the Chesapeake Bay. Hyperspectral instruments measure reflected light with much greater spectral resolution than the multispectral instruments currently deployed on ocean-observing satellites. Increased spectral resolution allows for better approximation of phytoplankton concentrations in optically complex waters. This research seeks to test optical inversion algorithms designed for turbid waters like the Chesapeake Bay. By pairing in situ measurements of chlorophyll with electromagnetic spectrum measurements, we determined the most accurate algorithms for use in the Chesapeake Bay. These algorithms can then be employed in future remote sensing studies to yield accurate chlorophyll measurements in fine temporal, and spatial time scales.

Document Type
Thesis

Distinguished Thesis
Yes

Degree Name
Bachelor of Arts (BA)

Department or Program
Biology

First Advisor
Lynn Westley

Second Advisor
Greg Silsbe, University of Maryland, Center for Environmental Science

Third Advisor
Scott Schappe

Fourth Advisor
Karen Kirk

Subject Categories
Biodiversity | Biology | Marine Biology

LAKE FOREST COLLEGE

Senior Thesis

Improving estimates of phytoplankton populations in the Chesapeake Bay using hyperspectral radiometers

by

Max Spehlmann

April 6, 2017

The report of the investigation undertaken as a
Senior Thesis, to carry two courses of credit in
the Department of Biology.

_____	_____
Michael T. Orr Krebs Provost and Dean of the Faculty	Lynn Westley, Chairperson
	_____
	Greg Silsbe University of Maryland, Center for Environmental Science
	_____
	Scott Schappe
	_____
	Karen Kirk

Abstract:

In coastal and estuarine waters, high turbidity and land interference severely diminish the utility of satellite data. This study tested the accuracy of hyperspectral inversion algorithms to better resolve chlorophyll *a* estimates in the Chesapeake Bay. Hyperspectral instruments measure reflected light with much greater spectral resolution than the multispectral instruments currently deployed on ocean-observing satellites. Increased spectral resolution allows for better approximation of phytoplankton concentrations in optically complex waters. This research seeks to test optical inversion algorithms designed for turbid waters like the Chesapeake Bay. By pairing *in situ* measurements of chlorophyll with electromagnetic spectrum measurements, we determined the most accurate algorithms for use in the Chesapeake Bay. These algorithms can then be employed in future remote sensing studies to yield accurate chlorophyll measurements in fine temporal, and spatial time scales.

This thesis is dedicated to my mom who reminds me to always look at the big picture.

Acknowledgments:

First and foremost, I would like to thank Dr. Lynn Westley for her excellent guidance and positive can-do attitude. Dr. Westley was a great thesis mentor, and through her tutelage, I am wholly confident in my ability to continue along a career path involving academic research. Dr. Greg Silsbe of Horn Point Labs deserves substantial recognition as well for his outstanding mentorship throughout the summer, and for his continuing support throughout the academic year. I was lucky enough to be able to go back to Horn Point over fall break to collect more data thanks to Dr. Westley. Likewise, the biology department at Lake Forest College helped fund my conference attendance at the Association for the Sciences of Limnology and Oceanography (ASLO) annual conference in Honolulu, Hawaii. The Rocky Mountain Biological Lab and Maryland Sea Grant also provided funding. In Hawaii, I presented this research and had the opportunity to see researchers involved in ocean remote sensing work from around the world, an opportunity for which I am very grateful.

The physics department of LFC also warrants special acknowledgement. Dr. Kash often entertained questions unrelated to his courses to help me understand the optical aspects of this research. Dr. Schappe also lent his expertise in helping me to understand the workings of the optical equipment. Dr. Frank lent her statistical expertise for the analysis section. My thanks go out to Dr. Menke as well for helping me shape the course of my studies at Lake Forest College. Through Dr. Menke's advising, I was able to effectively take advantage of all the fantastic resources and professors which call Lake Forest College their

own. Throughout the process of putting this work together, I have ever more strongly realized that I too am proud to call Lake Forest College my own.

Table of Contents:

Introduction:

Overview

Ecological research has been greatly served by the advent of remote sensing technology in the 1960's. Remotely sensed data are becoming ever more prevalent as new technologies and new mathematical techniques to use these technologies emerge. My research centered on using new technology to better quantify levels of phytoplankton in the Chesapeake Bay, the largest estuary in the United States. To appreciate the relevance, and importance of this research, I will briefly describe the role of the world's oceanic ecosystems in the global carbon cycle. I will describe the biological solubility pump, which accounts for two thirds of the total carbon exported from surface waters to the deep ocean. This will be followed by a brief description of estuarine ecosystems, which link riverine systems to oceanic environments. Because of the importance of phytoplankton on the biological solubility pump in the world's oceans and on the primary production (a gross measurement of inorganic carbon fixed into organic molecules) of estuaries, I will evaluate the growing body of scientific research on phytoplankton population dynamics. Next, I will describe the Chesapeake Bay in detail, and define the current state of its health. I will then discuss the way in which ecosystem level measurements are made using remote sensing. These techniques are currently robust in oceanic ecosystems, but lack accuracy and consistency in estuaries, for reasons I will elucidate. Hyperspectral radiometers are replacing multispectral radiometers because of their higher spectral resolution. I will discuss the development of inversion algorithms designed

specifically for hyperspectral radiometers, and finally delve into my research, which sought to test inversion algorithms designed for the Chesapeake Bay.

Carbon cycling in the world's oceans

Throughout the Earth's history, the world's oceans have played a crucial role in global climate cycles (Riebesell 2009, Falkowski *et al.* 2009, Sutton and Hodson 2005). Capable of storing 1,000 times more heat than the continents, oceans are the primary drivers of heat transport throughout the globe (Riebesell 2009). Because of their impact on wind-driven atmospheric currents, ocean currents are responsible for many decadal climate patterns, such as the warm summer months in North America and Northern Europe (Sutton and Hodson 2005).

The world's first life forms evolved in oceans millions of years before continental plates emerged (Canfield 2005). The evolution of oxygen producing organisms 2.4 billion years ago was arguably the most important evolutionary event since the first nucleotides became self-replicating (Canfield 2005). Oxygen is the principle reducing agent used by life on Earth. From their inception until 251 million years ago. Cyanobacteria were the principal producers of Oxygen until more complex taxas of aquatic life evolved (Flores and Herrero 2008). The beginning of the Mesozoic period (251-65 mya) saw the radiations of dinoflagellates, coccolithophorids and diatoms, however cyanobacteria continue to play a critical role in marine ecosystems to this day, especially in oceanic gyres (Flores and Herrero 2008). Collectively, these aquatic photoautotrophs are known as phytoplankton, from the latin 'phyto,' meaning light, and 'plankton,' meaning wanderer (Kirk 2011). Broadly speaking, phytoplankton are microscopic plants that convert radiant solar energy into chemical energy using specialized light capturing pigments. Phytoplankton principally rely on chlorophyll *a,* but may

use a suite of other light capturing pigments as well (Kirk 2011). Besides their contribution to maintaining atmospheric oxygen concentrations, phytoplankton play a critical role in the biological carbon pump of the world's oceans.

Atmospheric CO_2 is exchanged rapidly between terrestrial and oceanic ecosystems (Volk and Hoffert 1985). The relative rates at which both reservoirs exchange gases with the atmosphere effectively determine the overall rate of change of atmospheric CO_2 (Falkowski *et al.* 2009). The world's oceans represent a pool of 38,400 gigatons (Gt) of carbon, compared to the terrestrial biosphere which pools about 2,000 Gt of carbon (Toggweiler *et al.* 2003). Compared to the atmosphere, the world's oceans contain 50 times the amount of dissolved inorganic carbon (DIC) (Plattner *et al.* 2001). carbon is exchanged much more quickly with the oceanic reservoir than the terrestrial reservoir (Plattner *et al.* 2001). Because of this quick exchange time, on millennial scales, oceans determine atmospheric CO_2 concentrations: Atmospheric CO_2 concentrations do not determine oceanic CO_2 concentrations (Falkowski *et al.* 2009).

Atmospheric CO_2 is continuously exchanged with the ocean surface; therefore, the ocean surface rapidly equilibrates with the atmosphere (Riebesell *et al.* 2009). Once dissolved in oceans, DIC may follow one of three paths. It may become bicarbonate, and eventually sink below 100 meters where it cannot exchange with the atmosphere (a process known as export), or it may be incorporated into organic molecules by phytoplankton. I will briefly expound on each of these three processes.

Upon dissolution of CO_2, carbon forms a weak acid that reacts with carbonate ions and water to form bicarbonate (Hedges 1992). This efficacy of this buffer system to absorb inorganic carbon is dependent on the addition of cations from weathering rocks, which is an extremely slow process (Hedges 1992). Because the rate of CO_2 emitted from humans is increasing much more rapidly than the addition of cations, global oceans are becoming increasing acidic and less efficient absorbers of CO_2 (Plattner *et al.* 2001). A further discussion of the changing global oceans is discussed later in this section.

Vertical mixing is the process by which CO_2-saturated ocean water is exported to depth and is no longer able to exchange with the atmosphere. The two processes that govern this phenomenon are known as the solubility pump and the biological pump (Volk and Hoffert 1985). Because colder, more saline water has a higher solubility for CO_2, the northern latitudes absorb more CO_2. During the spring and fall turnovers, the dense surface waters, and all the CO_2 therein, are exported to depth and effectively stored in the deep ocean carbon sink. It may take decades to several hundred years for the deep ocean to reemit the stored carbon (Riebesell *et al.* 2009). Climate models suggest that as oceans warm in the coming decades, increasing stratification of the water column will prevent vertical mixing, and therefore diminish the ability of the solubility pump to absorb atmospheric carbon (Sarmiento and Le Quere 1996). Increasing oceanic stratification will also weaken currents and will likely have significant impacts on global weather patterns (Riebesell *et al.* 2009). The solubility pump accounts for roughly one third of all DIC export.

The biological pump accounts for the export of two thirds of DIC in the world's oceans (Riebesell *et al.* 2009). The biological pump begins with photosynthesis by phytoplankton, a process that uses DIC and therefore lowers the partial pressure of CO_2 in the photic zone (the depth to which light energy penetrates) (Falkowski *et al.* 2000). 25% of the carbon fixed by phytoplankton is exported to the aphotic zone (the depth to which no light reaches), where it is oxidized by heterotrophic organisms, mostly prokaryotes (Falkowski *et al.* 2000). The export of carbon by phytoplankton accounts for between 11 and 16 Gt of carbon per year and keeps atmospheric CO_2 concentrations 150 to 200 parts per million (ppm) lower than they would be in the absence of phytoplankton (Falkowski *et al.* 2000). Because of its ubiquity in all forms of life, the carbon cycle is closely linked to biological activity.

Net primary production (NPP) is a measure of the atmospheric CO_2 or DIC which is fixed into organic molecules by primary producers and therefore available to heterotrophic organisms. Specifically it is the rate at which primary producers fix carbon (gross primary production) minus the rate at which primary producers respire inorganic carbon (McGuire *et al.* 1997). Beyond their importance in the carbon cycle, photosynthesis by marine organisms produces between 30 and 60 petagrams (1 Pg = 10^{15} g) of organic carbon per year (Smith and Hollibaugh 1993), which accounts for upwards of 40% of the total NPP on Earth (Schlesinger 1991). The responses of NPP to anthropogenic carbon emissions are of concern because humans derive all their food, fuel and fiber from primary producers (Vitousek *et al.* 1986). NPP measurements are becoming

more accurate and detailed as remote sensing technologies improve. I will discuss these technologies further in a future section.

The oceans have already absorbed an estimated 50% of anthropogenic CO_2 (Riebesell 2009). However, negative feedback loops have lowered the efficacy of the carbon pumps to export carbon to the deep ocean. The rate at which carbon export will decrease, and the implications thereof, is still uncertain (Bopp *et al.* 2001). I will expound upon the most pertinent negative feedbacks currently in effect.

The arctic ocean surface layers have been warming and freshening, reducing their solubility of CO_2, and weakening global currents that contribute to vertical mixing in other regions of the globe (Gregory *et al.* 2005, Curry and Mauritzen 2005). The weakening currents will decrease the oceanic uptake of carbon by 3-20%, and the reduced solubility of warmer ocean waters will reduce the oceanic uptake of carbon by 9-15% by the end of the 21st century (Riebesell 2009). The biological carbon pump is much more difficult to model, and scientists are unsure about how phytoplankton populations will respond to increasing ocean temperatures, decreasing salinity, and decreasing mixing (Gregory *et al.* 2005). Warmer temperatures tend to favor the growth of heterotrophic grazers (zooplankton that eat phytoplankton), and reduced mixing will undoubtedly limit the ability for phytoplankton to grow, however it is possible that the increasing DIC in the photic zone will favor the growth of some phytoplankton taxa with inefficient CO2 acquisition pathways (Riebesell 1993). Although governed by the same physical processes, estuaries are characterized by a much higher degree of primary productivity and a much lower degree of DIC export than oceans.

Carbon cycling in Estuaries

Although marine research has typically centered on the open ocean, coastal environments and estuaries are extremely important drivers on the global carbon cycle (Mcleod *et al.* 2011). Although they may be inundated with water for extended lengths of time, coastal salt marshes, mangrove forests, and seagrass meadows are considered terrestrial ecosystems by earth systems modelers. These ecosystems, so called “blue carbon reservoirs” have a high capacity for sequestering carbon. Despite their relatively low land cover, coastal ecosystems bury levels of carbon comparable to those of terrestrial forests (Mcleod *et al.* 2011).

Estuaries are considered oceanic ecosystems by earth systems modelers, and they are typically included in the carbon budget of oceans. Estuaries do not export carbon to the deep ocean: instead, they support a high degree of net primary productivity (NPP) and function to release carbon into the atmosphere (Cloern *et al.* 2014). In fact, the high respiration rates in estuaries reduces the total calculated oceanic global CO_2 uptake by 12% (Borges 2005). Organic carbon is cycled more efficiently in estuarine environments and coastal oceans (Smith and Hollibagh 1993). Several factors likely impact this trend, most importantly, estuarine systems receive high degrees of nutrient influx which foster the concentrated growth of phytoplankton, and are subject to periodic mixing episodes which help to redistribute nutrients and organic matter (Smith and Hollibagh 1983). Because of the magnitude of human perturbation to riverine systems which eventually flow into estuaries, the degree to which human activity is altering the carbon dynamics of estuaries is most likely more severe for

estuaries than the open ocean (Holligan and Reiners 1992). The need for large-scale ecosystem measurements is therefore difficult to overemphasize.

Quantifying the extent to which estuaries contribute to global primary production and the release of carbon, is obfuscated by their high degree of environmental variability. Estuary nutrient availability and stratification are affected by the following: the seasonal upwelling of deep, nutrient-rich water from oceans; the seasonal influx of warm, freshwater from the continental watershed; wind patterns, tidal fluctuations, and long-term ocean current oscillations; global climate change, and sea level rise; and the abundance of benthic organisms, and submerged aquatic vegetation (SAV), which regulate nutrient recycling (Cloern *et al.* 2014). A study of the net primary production of any ecosystem begins with the base of the food web. As in their oceanic counterpart, phytoplankton account for most of the primary production in estuarine environments, therefore in the next section I will examine the role of phytoplankton in estuarine environments in further detail.

Primary production in estuaries

Unlike the open ocean, very little carbon is exported to depths in estuaries, most is eventually respired back into the atmosphere by heterotrophs (Borges 2005). Because of their position at the base of the estuarine food web, phytoplankton are the most important drivers of the carbon cycle in estuaries. Phytoplankton enrich dissolved organic carbon with lipids and nitrogen creating easily assimilated energy sources for heterotrophic organisms. Most (~90%) of the organic matter produced by phytoplankton is consumed or decomposed to support heterotrophic metabolism (Duarte and Cebrian 1996). This stands in

contrast to organic carbon from land runoff, which is typically low in nutrients and is primarily metabolized by microbial decomposers (Sobczak et. al 2005). Vascular plants and macroalgae also produce a significant amount of organic matter. However, only 20% of their organic matter is consumed by heterotrophs, the majority is recycled back into CO_2 by decomposers, or exported to sediment (Cebrian 1999). Understanding phytoplankton population dynamics in estuaries will allow for a better understanding of the total amount of carbon being emitted into the atmosphere from estuaries. Phytoplankton population dynamics are best understood in ocean ecosystems, therefore in the next section I will describe the current understanding of phytoplankton dynamics in the world's oceans.

Global phytoplankton population dynamics

To understand the long-term patterns of phytoplankton population variation, and to better tease apart anthropogenic influences from natural cycles, oceanic researchers have been expanding and modifying the current view of phytoplankton growth dynamics. Phytoplankton populations are characterized by periods of stability interspersed with periods of rapid growth and subsequent die offs, commonly referred to as "blooming." The traditional view of phytoplankton blooms has centered on "bottom-up" controls of phytoplankton growth; namely the influence of nutrient and light limitation of phytoplankton growth. This hypothesis also maintained that the rapid growth of phytoplankton depended on an ecological disturbance event, e.g., the decreasing stratification of the water column in the spring and fall, to begin acceleration phytoplankton division rates. This view pervaded the literature of biological oceanography until a number of large-scale iron-enrichment studies were conducted in the 1990s (Behrenfeld

2010, Boss and Behrenfeld 2010, Behrenfeld *et al.* 2013). The emerging consensus among biological oceanographers is that top-down (i.e., higher trophic level interactions between autotrophic phytoplankton and heterotrophic zooplankton) controls must be accounted for in order to explain phytoplankton blooming (Behrenfeld 2014). This hypothesis was greatly bolstered by a handful of key, turn-of-the-century oceanographic expeditions.

Four recent experiments artificially added iron to iron-limited areas in the world's oceans (Boyd *et al.* 2004, Tsuda *et al.* 2003, Coale *et al.* 1996, Boyd *et al.* 2000). In all four of the experiments, phytoplankton began to grow exponentially after 4-5 days. Growth began to slow and then decrease linearly in about a week (Boyd *et al.* 2004, Tsuda *et al.* 2003, Coale *et al.* 1996, Boyd *et al.* 2000). Interestingly, phytoplankton growth stopped rising before the depletion of iron. Because neither light nor nutrients were limiting phytoplankton growth in their study area, their growth must have been checked by grazers (Landry *et al.* 2000, de Baar *et al.* 2005).

Further evidence for the importance of top-down regulation on phytoplankton growth was found upon the taxonomic identification of the blooming species of phytoplankton. Initially many diatom species were present in the study areas, however, in all four experiments, the blooming population was composed of only one species of phytoplankton. The blooming species not consistent among the four study sites. Because most diatom species experience similar stimulation due to iron enrichment and have similar division rates, the only logical explanation appeared to be trophic web interactions: the blooming

population of diatoms must have been the species that experienced the least predation (Behrenfeld 2014).

The dynamics of the lower levels of marine ecosystems are complex. Both phytoplankton and zooplankton display a dizzying array of morphologies which have implications for their ability to prey upon or avoid predation successfully. Furthermore, the life histories of marine creatures are complex and depend upon food availability, and the physical characteristics of their environment (Verity *et al.* 2002). Therefore, it is likely that one species tends to dominate in blooming populations because that population happened to have physical traits that prevented its consumption by zooplankton (Mariani *et al.* 2013).

To add further credence to the importance of the top down hypothesis, ecosystem modelers began to incorporate a carnivore predation term into their ocean models as a density dependent loss rate (Calber and Landry 1999). When combined with “bottom up” information, e.g., mixed layer depth, ocean temperature, light attenuation, the ocean models began to satisfactorily predict both the magnitude and intensity of oceanic phytoplankton blooms within a broad spatial scale (Behrenfeld 2014). Because these models now take into account the ecosystem feedbacks between phytoplankton and their grazers, scientists can now predict both the time and place of major phytoplankton blooms in the global oceans. Furthermore, a more robust bloom hypothesis has been proposed which blends aspects of the previous bottom down hypothesis to the top down hypothesis: The current consensus is that phytoplankton blooms form because of an ecosystem interruption (e.g., rapid nutrient influx from storm events, seasonal water column inversion, freshwater intrusion) which causes phytoplankton growth

to decouple from predation and allow the formation of a bloom until grazers can regain high population levels (Anderson *et al.* 2010).

The above insights represent significant advancements the study of the biological carbon pump. However, a greater level of refinement is necessary in order to predict blooms in coastal and estuarine environments (Behrenfeld *et al.* 2013). Although the above research centered on phytoplankton populations in the open ocean, these findings no doubt play important roles in coastal and estuarine environments (Behrenfeld 2014). The impact that top down controls play in more productive environments is an active area of research.

Although worldwide, phytoplankton levels appear to be geometrically decreasing (Boyce 2010), levels have been markedly increasing in the Chesapeake Bay since at least the 1950's (Harding 1994). To date, little to no research has been done to elucidate the impacts of grazers on controlling blooms and hence impact the carbon cycle, in estuarine environments. The first steps in establishing a satisfactory ecosystem model must include more detailed information on phytoplankton population levels within fine spatial and temporal scales (Anderson *et al.* 2010 and Prowe *et al.* 2012). Only then can a more nuanced understanding of phytoplankton growth dynamics in estuaries be adequately characterized to predict when and where phytoplankton populations will bloom, as well as to understand which phytoplankton species will bloom. My research ultimately seeks to improve upon our understanding of phytoplankton populations in the Chesapeake Bay.

Phytoplankton dynamics in the Chesapeake Bay

The Chesapeake Bay is the largest estuary in the USA (Darrell 1998). It is almost 300 km long, with a relatively deep (20 to 30 m) and narrow (1 to 4 km) central channel confined by a sill at its inward end (Darrell 1998). Approximately half of the Chesapeake Bay's water supply originates from the Atlantic Ocean, while, the other half originates from its enormous (~166,530 km^2) watershed (Darrell 1998). Collectively, the Bay's three largest rivers, the Susquehanna, Potomac, and James Rivers, provide 80% of the freshwater flow into the bay (Darrell 1998). Strong river flow is the predominant driver of estuarine circulation: warm freshwater sits atop counter-flowing, dense sea-water and acts to retain particulate and dissolved materials in the Bay. Consequently, this circulation regime promotes long nutrient residence times (90 to 180 days) (Pritchard 1956; 1967). It also sets up well-defined stratification, which ultimately suppresses vertical nutrient exchange and isolates the deeper channel waters (Boicourt 1992). The level of the water column through which irradiant light energy penetrates is known as the euphotic zone (Martin 2014). Nutrients are cycled more efficiently in the euphotic zone of the Chesapeake Bay than the aphotic zone.

The primary drivers of nutrient and carbon cycling in the Chesapeake Bay are phytoplankton (Sobczak et. al 2005). Within the first ten meters of the water column, phytoplankton metabolize nutrients efficiently (Boicourt 1992). Phytoplankton species dynamics change both seasonally and on interannual timespans (Kemp *et al.* 2005). Although it is difficult to isolate seasonal variability from long-term changes, phytoplankton dynamics have been undergoing definite

changes since measurements began in the early 20th century (Kemp *et al.* 2005). Diatom species abundance has been declining relative to smaller dinoflagellates, cyanobacteria, and small flagellates (Zimmerman and Canuel, 2002). Because smaller taxa of phytoplankton are lower quality food sources for copepods and oysters, the taxonomic composition of phytoplankton holds implications for the entire Chesapeake Bay food web (Verity 1988).

Phytoplankton undergo predicable patterns of seasonal variation. Enhanced precipitation in the winter and early spring lead to high levels of available nutrients in the euphotic zone (Verity 1988). Consequently, a large bloom of centric diatom bloom occurs in the spring (Verity 1988). The blooming diatom population is eventually checked by a burgeoning zooplankton population composed of copepods and rotifers (Verity 1988). These species are then consumed by gelatinous predators such as ctenophores and medusa, and fish such as menhaden and blue herring (Verity 1988, Baird and Ulanowicz 1989). In the summer months, smaller species of phytoplankton tend to bloom, such as various species of dinoflagellates, picoplankton and small centric diatoms (Najjar *et al.* 2010). Overall, the food web of the Chesapeake Bay is complicated and not static in time; it is subject to a huge variety of exogenous inputs and environmental factors. Attempting to delineate cause and effect in the estuarine food chain is therefore extremely challenging (Verity 1988, Baird and Ulanowicz 1989). It is clear however that the influx of anthropogenic nutrients has been negatively affecting the health of the Chesapeake Bay.

Nutrient loading in the bay has undergone a marked increase since intensive agricultural operations began in 1850 (Darrell 1998). Phytoplankton

responsiveness to eutrophic conditions is not totally understood, but phytoplankton biomass and reproduction are clearly positively correlated with nutrient loading (Nixon 1992). Sellner *et al.* (1998) found that when sewage discharge into the Chesapeake Bay was screened of phosphorous, in the early 1970's, the frequency of the toxic cyanobacterium, *Microcystis aeruginosa* declined sharply (Sellner *et al.* 1988; Jaworski 1990). When eutrophic conditions persist, phytoplankton populations may bloom and cause direct harmful effects, including production of toxins, noxious discoloration, diminution of water clarity and floating mucilage (Kemp *et al.* 2005). As blooming populations die, their bodies are broken down by bacterial decomposers, which have a high demand for dissolved oxygen. Phytoplankton blooms, therefore, tend to increase hypoxia. Furthermore, large accumulations of phytoplankton shade submerged aquatic vegetation, which may contribute to their death as well as exacerbate hypoxia (Harding 1994). This drain in oxygen severely limits heterotroph respiration, and periodic, anoxic dead zones are becoming increasingly common (Kemp *et al.* 2005).

Although complex and changing rapidly, the Chesapeake Bay's food web is characterized by a high level of primary production, and abundant marine life (Cloern *et al.* 2014). Because of their position at the base of the estuarine food web, phytoplankton populations have implications on commercial fish and benthic invertebrate populations (Herman et. al,1999). To date, our knowledge of phytoplankton populations in the Chesapeake Bay is sparse in both temporal and spatial scales (Cloern *et al.* 2014). Remote sensing has the potential to provide

robust phytoplankton concentration data in the Chesapeake Bay. It has already been used extensively in the open ocean.

Measuring ecosystem-scale processes

Up until the 1980's, ocean research is conducted by means of discrete *in situ* measurements from research piers or vessels. The C^{14} tracer method was developed and tested by Steeman Nielson in 1952 to track the radioactive signal of carbon tracers throughout the ocean ecosystem (Longhurst *et al.* 1995). A great degree of methodological criticisms suggested that the tracer method tended to underestimate production rates, and this method largely fell out of favor as satellite-mounted radiometer data became more widely available (Longhurst *et al.* 1995). Costs of fuel and equipment also limited the spatial and temporal extent of data available for marine environments.

With the advent of satellite imagery in the late 1960's, scientists have been collating a vast database of ocean light data (Martin 2004). The MODIS camera aboard the AQUA satellite is used for remote sensing information in the open ocean (Martin 2004). This multispectral camera scans light in 6 discrete wavebands. From these wavebands, scientific institutions such as NASA and NOAA have created algorithms which invert light data into ecosystem parameters. Oceanographers have been refining data processing protocols to remove the effects of sun angle away from the nadir, wind-born water vapor, and scattering by atmospheric particles (Martin 2004). After processing, light data can be scaled to relevant ecosystem parameters, such as water depth, temperature, carbon biomass, and chlorophyll concentration (Silsbe 2016). The processed

light data can then be inverted into a biologically prevalent parameter such as NPP.

As stated above, one of the key goals of marine ecosystem modelers is to understand the biological carbon pump of the ocean, i.e., the process by which inorganic carbon is either exported to the deep ocean or made available for use by heterotrophic organisms via primary producers (Riebesell 2007). An understanding of this process is necessary to develop accurate accounts of the net primary productivity of the world's oceanic ecosystems. Currently, a great deal of uncertainty pervades oceanic NPP estimates: estimates range from 32 to 79 Pg C m^{-2} yr^{-1} (Pg C is petagrams of carbon) (Carr *et al.* 2006).

The Carbon, Absorption, and Fluorescence Euphotic-resolving (CAFÉ) net primary production model is the most advanced method for determining NPP. The model uses the light absorption attributable to phytoplankton to extrapolate their growth rate, μ. μ is then multiplied by the biomass of phytoplankton to yield NPP. Using this model, the current best-estimate for annual net primary production is 52.2 Pg C m^{-2} yr^{-1} (Silsbe 2016). Unfortunately, the strength of these models to estimate NPP in estuarine environments is limited due to high sediment loading which obfuscates the reflectance spectra and therefore diminishes the accuracy of ocean color inversion algorithms (Kirk 2011). The current best estimate of the NPP in the Chesapeake Bay stands at 50 g C m-2 yr (Kemp 1997). However, this estimate was created using data high inaccuracy relative to ocean measurements (Cloern *et al.* 2014). Furthermore, estuaries are dynamic and exhibit a large amount of temporal and spatial heterogeneity in production (Cloern *et al.* 2014), therefore greater spatial and temporal data

offered by new hyperspectral radiometers will greatly improve our understanding of these productive environments.

Hyperspectral Remote Sensing

Hyperspectral radiometers have broader spectral ranges and higher resolutions than multispectral radiometers. NASA is currently scheduled to launch the PACE satellite in 2020 which is the first satellite to be equipped with a hyperspectral radiometer (Martin 2004). The greater spectral detail will allow modelers to use reflectance information from more wavelengths to better differentiate the reflectance of phytoplankton from the reflectance of sediment. More accurate NPP estimates will be available for highly productive coastal waters and estuaries, such as the Chesapeake Bay. In this research, I focused on inversion algorithms designed to yield greater accuracy of chlorophyll levels in turbid environments. From accurate chlorophyll measurements, accurate phytoplankton concentration can be estimated. These estimates will better characterize the NPP of the Chesapeake Bay. In the next section, I will describe the process by which light data is inverted to ecosystem parameters.

Remote sensing inversion

Satellite mounted radiometers measure the light reflected from the surface of the Earth. Remote sensing reflectance, $R_{RS}(\lambda)$, is the upwelling radiance, $L_u(\lambda)$, normalized to the downwelling irradiance, $E_d(\lambda)$ (1).

$$R_{RS}(\lambda) = \frac{L_u(\lambda)}{E_d(\lambda)} \quad (1)$$

$R_{RS}(\lambda)$ is an apparent optical property of aquatic media: it depends on the unique absorbance and scattering functions of each component within the water column,

i.e., the inherent optical properties (IOPs) of the medium. The components of the aquatic medium remove energy from a light beam as it propagates through the water column. Components may either scatter light energy or absorb light energy (Bukata 1995). Under a simplified model, the pertinent components of the water column are Colored Dissolved Organic Molecules (CDOM), phytoplankton, sediment and water itself.

Scattering occurs when light causes electrons to oscillate and reradiate light at a different angle (Meyer-Arendt 1972). The loss of light energy due to scattering is dependent on the incident angle of the light beam, and component size and composition (Bukata 1995, Dickey *et al.* 2011). The variability of scattering due to component size, composition, and incident light angle makes accurately describing scattering difficult, therefore improved scattering measurements will have the largest impact on the optical closure of reflectance inversion algorithms (Tzortziou 2007). Total backscattering, $b_b(\lambda)$, is the sum of the backscattering due to phytoplankton, $b_\phi(\lambda)$, particulate matter, $b_{pm}(\lambda)$, and water, $b_{bw}(\lambda)$ (backscattering due to CDOM is negligible) (Equation 2).

$$b_b(\lambda) = b_\phi(\lambda) + b_{pm}(\lambda) + b_{bw}(\lambda) \quad (2)$$

Light absorption occurs when light of a particular frequency passes through matter, sets electrons oscillating, and is not reemitted (Meyer-Arendt 1972). Light absorption is dependent on the unique resonance frequencies of molecules, and not the angle of incident light, therefore it is more easily predictable than scattering (Stomp *et al.* 2007 and Martin 2007). Total

absorbance, $a(\lambda)$, is the sum of the absorbance due to phytoplankton, $a_{\phi}(\lambda)$, pure water, $a_w(\lambda)$, CDOM, $a_{CDOM}(\lambda)$, and particulate matter, $a_{pm}(\lambda)$ (Equation 3).

$$a(\lambda) = a_w(\lambda) + a_{\phi}(\lambda) + a_{CDOM}(\lambda) + a_{pm}(\lambda) \quad (3)$$

As stated earlier, under a simplified model, the scattering and absorption of these three aquatic constituents account for all of changes in light energy as it is transmitted through the aquatic medium (Mobley 2014). Thus, $R_{RS}(\lambda)$ is an emergent property of the unique absorption and scattering properties of every element within the water column (Equation 4).

$$R_{rs}(\lambda) = \frac{b_b(\lambda)}{b_b(\lambda) + a(\lambda)}. \quad (4)$$

CDOM (also referred to as gelbstoff, yellow substance, and chromomorphic dissolved organic matter) is derived from several sources, both terrestrial and marine (Martin 2014). The exact constituents of CDOM vary between environments (Martin 2014). Terrestrial CDOM is typically composed of decaying vegetable matter, which decompose into humic and fulvic acids (Martin 2014). Oceanic CDOM is composed of dead phytoplankton and zooplankton fecal pellets (Roesler *et al.*,1989). The absorption of CDOM across wavelengths follows a logarithmic decay. CDOM tends to be the dominant absorber of light until 500 nm, at which point water is the dominant absorber (Kirk 2011). CDOM's contribution to scattering tends to be negligible in comparison to particulate matter (Kirk 2011).

Particulate matter is tidally stirred sediment, eroded soil, or detritus (Moore 1999). Land runoff is generally much higher in overgrazed pastures, and logged

forests (Kirk 2011). The exact amount of soil eroded is also dependent on the vegetation type, the soil composition, the slope of the land, and the intensity of rainfall (Kirk 2011). Once in water, particles in suspension become sedimented at varying rates. The amount of time particles remain suspended depends on the electrolyte concentration within the water body (Kirk 2011). Particulate matters absorb very little across all wavelengths (Kirk 2011). The presence of particulate matter substantially increases scattering in inland water bodies (Nolen 1985). The degree to which particles scatter light is both a property of particle size and particle concentration, however particle size has been shown to be much more important on scattering intensity, with larger particles tending to scatter more light than smaller particles (Kirk 1985). In turbid environments, the wavelength dependence of scattering by particulate matter can be described by a power law: higher wavelengths are scattered more than lower wavelengths (Morel and Prieur 1977). In turbid waters, the ratio of light scattered at 700 nm to 300 nm was found to be 1.84 (Morel and Prieur 1977). Scattering of light by larger particles exhibits increasing wavelength dependence than scattering by small particles (Martin 2014).

Phytoplankton capture light energy in special photo-system complexes to reduce inorganic carbon into organic molecules (Kirk 2011). Light absorption due to phytoplankton depends on the exact pigment types expressed, and their cellular size and composition (Kirk 2011). Because Chlorophyll molecules absorb light in the red and blue wavelengths, absorption by phytoplankton exhibit two distinct peaks in these wavebands (Kirk 2011). In his 1998 study, Volten found

that the backscattering of light attributable to phytoplankton was had negligible impacts on RRS(λ) measurements (Volten 1998).

The exact way in which water absorbs light depends upon the three vibrational modes of the water molecule (Stomp *et al.* 2007). Unlike most substances the blue color of pure water is due to molecular vibrations and not electron interactions (Dickey 2011). Water is primarily an absorber, and pure water tends to scatter much less light than particulate matter (Volten 1998). The wavelength dependence of water absorbtion is a well-established function of temperature and salinity (Silsbe, pers. comm.).

Because of the high degree of backscattering attributable to particulate matter, site-specific algorithms have been developed to isolate chlorophyll concentration information in the turbid waters (henceforth referred to as “case II” waters). These algorithms use features in the reflectance spectra to isolate IOPs of equations 2 and 3. In my study, I used algorithms which inverted RRS(λ) into a $a_{\phi}(\lambda)$, from which the concentration of Chlorophyll *a* can be extrapolated based on measured constants.

Case I vs. Case II remote sensing

In the open ocean (case I waters), phytoplankton tend to be the dominant non-water absorbers of radiation (Martin 2015).Therefore, phytoplankton light absorbance can be easily ascertained and extrapolated into phytoplankton concentration data by simply taking a ratio of the light reflected in green wavelengths to the light reflected in the blue wavelengths (Martin 2014). However, in estuarine and coastal waters (case II waters) CDOM and sediment

tend to obfuscate the reflectance spectrum (Tzoztiou 2007). Therefore, generating reliable phytoplankton concentration estimates in case II waters, with large riverine inputs of dissolved and suspended particulate matter, is difficult (Moreno-Madriñán and Fischer 2013). Typical case II inversion algorithms in utilize the reflectance minimum at 672 nm (Figure 1). Chlorophyll *a* exhibits strong absorption in this red waveband, therefore if the light intensity absorbed by CDOM and scattered by sediments are removed from the RRS(λ) at this waveband, accurate retrievals of phytoplankton absorbance are possible (Tzortziou 2007). The absorption of phytoplankton can then be scaled to phytoplankton concentrations using standardized relationships developed by researchers (Kirk 2011). Because of the variability of backscattering by particulate matter in the Chesapeake Bay, researchers have been working to refine spectral inversion algorithms which can accurately measure chlorophyll a absorbance, and consequently phytoplankton concentration, in all parts of the bay (Tzortziou 2007).

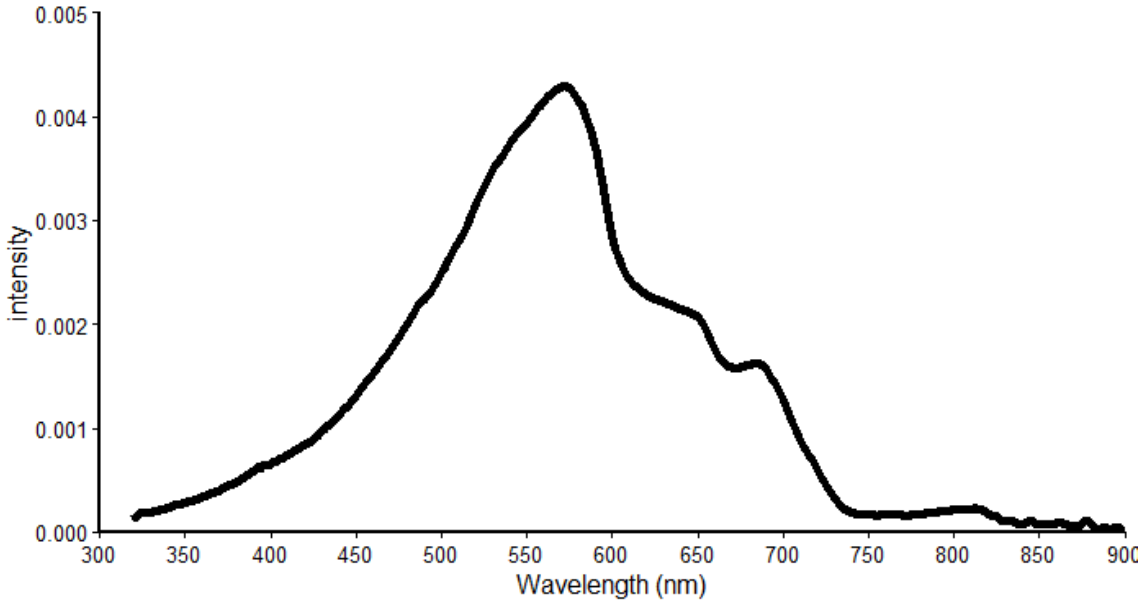

FIG. 1. Example reflectance spectrum from a case I water. Note the distinct peak at 555 nm, and the minimum at 672nm, both of which are attributable to phytoplankton.

I evaluated the accuracy of four of these inversion algorithms using *in situ* measurements of chlorophyll paired with electromagnetic spectrum data taken by hyperspectral radiometers. More accurate and more frequent chlorophyll measurements will shed light on the health of the bay, and allow for better understanding of the role estuaries play in the global carbon cycle.

Methods:

Study Site

The Choptank River is situated in the northern half of the Chesapeake Bay in the Delmarva Peninsula in Maryland. It lies entirely in the Atlantic Coastal Plain (Darrell 1998). The Choptank River has a drainage basin encompassing approximately 2,059 km^2 (Darrell 1998). In general, the Choptank Basin has been characterized as a poorly drained basin (Darrell 1998). Poorly drained areas tend to have lower nutrient concentrations than better drained areas (Darrell 1998). However, during wet years a rapid influx of nutrients can rapidly alter rates of nutrient loading (Pluta 2015).

Within the Choptank's watershed, agricultural land use (62%), mostly wheat, soybean, and corn, dominates (Sutton 2010). Forests are also abundant in the watershed, making up 26% of land cover (Fisher et al 1998). About half of all forests in the watershed are established riparian forests. Urban and developed areas make up 5% of land use, although this number is expected to rise as urban construction projects continue (Fisher et al 2006). The Choptank is a relatively small tributary to the Chesapeake, contributing 1.2% of the freshwater flow into the Chesapeake Bay (Darrell 1998). In comparison, The Susquehanna River, the largest tributary, contributes 52% of freshwater flow into the Chesapeake (Darrell 1998). Along the river, a pronounced salinity gradient exists: upriver salinity may be as low as 2.5 parts per thousand, whereas downriver, salinity may be as high as12.5 ppt (Weinberg 2008). A marked turbidity gradient also exists: the mouth of the river is much clearer than waters upstream (Pluta 2015). In order to capture

the spatial heterogeneity of chlorophyll *a* levels and optical properties, my transect covered about one third of the total distance of the Choptank River.

Collection dates

Data were collected throughout the summer and fall of 2016. A ten station transect was sampled from the Choptank river on five different days (Fig. 1). Stations were selected to span a large optical gradient. Additional sampling sites included seven stations on the northern Choptank and Tuckahoe Rivers (Fig. 2). At each station, data were collected using a floating rig with two vertically-oriented radiometers. Discrete water samples were also collected from the surface of the water.

Radiometric measurements

Radiometric measurements were made from a surface float, consisting of two hyperspectral radiometers (Trios Ramses, Rastede, Germany), which simultaneously measured $L_u(\lambda)$ and $E_d(\lambda)$. Each radiometer has a wavelength range of 320 to 950 nm, and a spectral resolution of 3.3 nm. The downwelling sensor measures the irradiant light field as well as the sensor inclination from the vertical. The upwelling sensor measures the light radiance (sensor A in figure). Following the skylight blocking approach outlined in Lee et. al, (2013), a black cone was attached to the upwelling sensor to remove light scattered from the atmosphere (sensor B in figure).

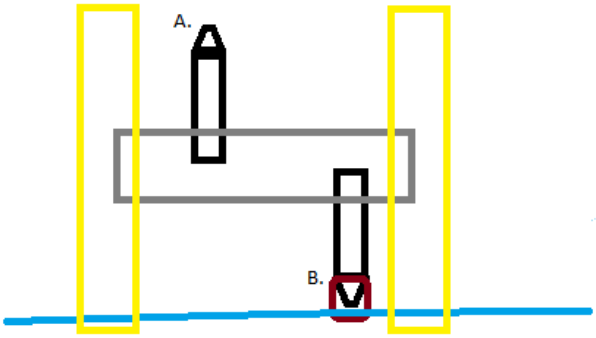

FIG. 2. Float schematic where A. is the downwelling light sensor and B. is the upwelling light sensor shown with a light-blocking cone (maroon circle).

The float was lowered into the water from the side of the sampling craft. Care was exercised to ensure the upwelling sensor was never completely below the water column. Before sampling began, the boat was reversed away from the float, to ensure that the sensor was not covered by the shadow of the vessel. The radiometric float was deployed for approximately five minutes with a sampling interval of ten seconds.

Quality control

Downwelling irradiance was divided by upwelling radiance to determine $R_{RS}(\lambda)$ (Equation 1). $R_{RS}(\lambda)$ is determined primarily by the IOP's present in the water column, however it is still sensitive to wind speed, viewing angle, and the presence of clouds. To standardize IOP estimation, optical inversion algorithms have been developed assuming perfect light conditions, i.e., when the Earth is at its mean distance from the sun, the sun is at its zenith angle and in the absence of any atmospheric loss (Morel and Gentili 1996). Ideally, the upwelling sensor would measure only light emitted from one discrete angle (the radiance), however wind speed scatters light from the sea surface and therefore the sensor

may not viewing one discrete path of light (Mobley 2000). Thus, prior to averaging the $R_{RS}(\lambda)$ intensity values, and following the methodology outlined in Ruddick et. al 2006, we included only spectral measurements taken from the sensors with a tilt angle less than five degrees from the vertical. Additionally, it has been found that in order to minimize the sea surface reflectance factor, light measurements should be taken on cloudless days (Mobley 2000). Therefore, we removed spectra with abnormally low downwelling irradiance values at 550 nm as this was most likely due to a cloud passing (Ruddick *et al.* 2006).

Fluorometry

Chlorophyll *a* concentrations were determined fluorometrically following the methods of Strickland and Parsons (1972). *In situ* water samples were filtered using GE filters with a pore size of .7 microns. Each filter was then placed in a scintillation vial filled with 20 ml of 90% acetone for 24 hours. Next, a Fluoromax 3 fluorometer (Horiba, New Jersey) was set to transmit light at 440 nm and read emission at 680 nm. The emission values of the extracted chlorophyll were read and then corrected for machine noise. N.B. for the final two transects, a Turner fluorometer (San Jose, CA) set to the same settings as the Fluoromax fluorometer was used.

In order to ascertain chlorophyll *a* levels from the emission intensity value, we created a standard curve from known concentrations of pure chlorophyll *a* and fit the emission values to the standard curve after correcting for different filtered water volumes.

Data analysis

Paired measurements of $R_{RS}(\lambda)$ and chlorophyll concentration allowed us to test the accuracy of four optical algorithms that scale $R_{RS}(\lambda)$ to chlorophyll *a* concentration. Table one outlines the algorithms tested, all algorithms are named according to their reference unless stated otherwise.

Table 1. Short description of the four spectrum inversion algorithms tested.

Model Type	Reference	Algorithm Summary
Empirical	O'reilly *et al.* 2000	Two waveband model developed for the open ocean referred to as OC4V4
Empirical	Gons 1999	Two waveband model developed specifically for turbid waters
Empirical	Ruddick 2001	Improved, dynamic two waveband model
Semi-Analytical	Gitelson 2005	Three waveband model, tuned to multiple case II water datasets.

Because there was uncertainty associated with both the model predicted chlorophyll concentration and the actual chlorophyll concentration measured via fluorometry, a type two linear regression was used in comparing the model results to the lab measured results.

A type II regression was used because there was uncertainty in both the predicted chlorophyll *a* estimates and the fluorometer-derived chlorophyll measurements (Brewin *et al.* 2012). In order to capture the systematic errors attributable to each algorithm, I plotted the mean normalized bias (MNB) where,

$$MNB = mean(100 * \frac{chla_{pred} - chla_{meas}}{chla_{meas}}). \quad (5)$$

To capture the random error attributable to each algorithm, I calculated the normalized root mean square error (NRMSE) where,

$$NRMSE = stDev(\left(100 * \frac{chla_{pred} - chla_{meas}}{chla_{meas}}\right). \quad (6)$$

Following the protocol of Brewin *et al.* (2012), I ran a Pearson correlation coefficient (*r*) test to determine whether each individual algorithm performed significantly better than the average algorithm performance. All of the statistics were carried out in R using the hydroGOF and lmodel2 packages. Plots were made using ggplot2.

Results:

Qualitative:

The following plot (Fig. 3) was created in order to optically characterize the transect. The underlying map was created in Google Earth. Figure 3 clearly shows an optical gradient in the reflectance spectra. As the stations moved further and further upstream, the reflectance in the ranges of 500-650 nm increases at every point. The slope of the spectra line at these points also decreases, indicating that the water is becoming browner.

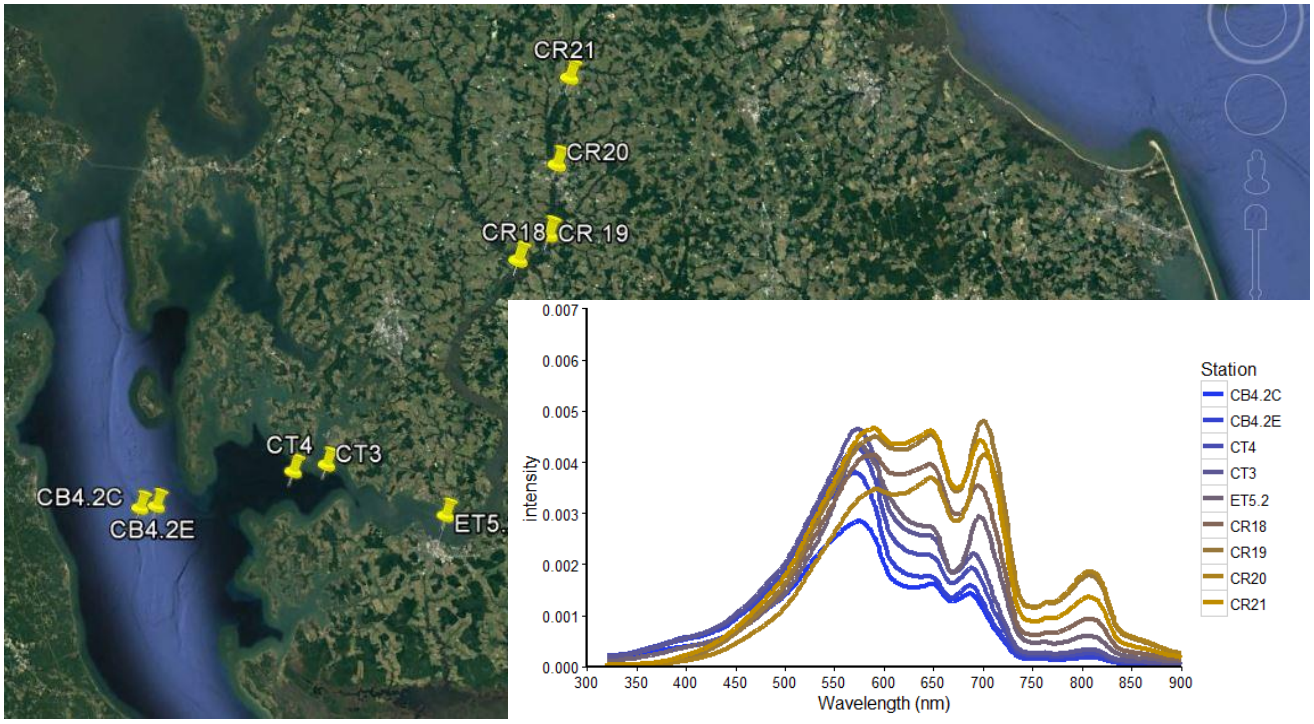

FIG 3. Reflectance spectra for transects run on 8/3 (CR18-CR21) and on 8/5. Stations were selected to clearly show the changing light spectra from downriver to upriver.

Quantitative:

The following graphs show the predicted chlorophyll *a* concentrations plotted against the lab measured chlorophyll *a* concentrations and the normalized bias for each algorithm. The combined data was N=61.

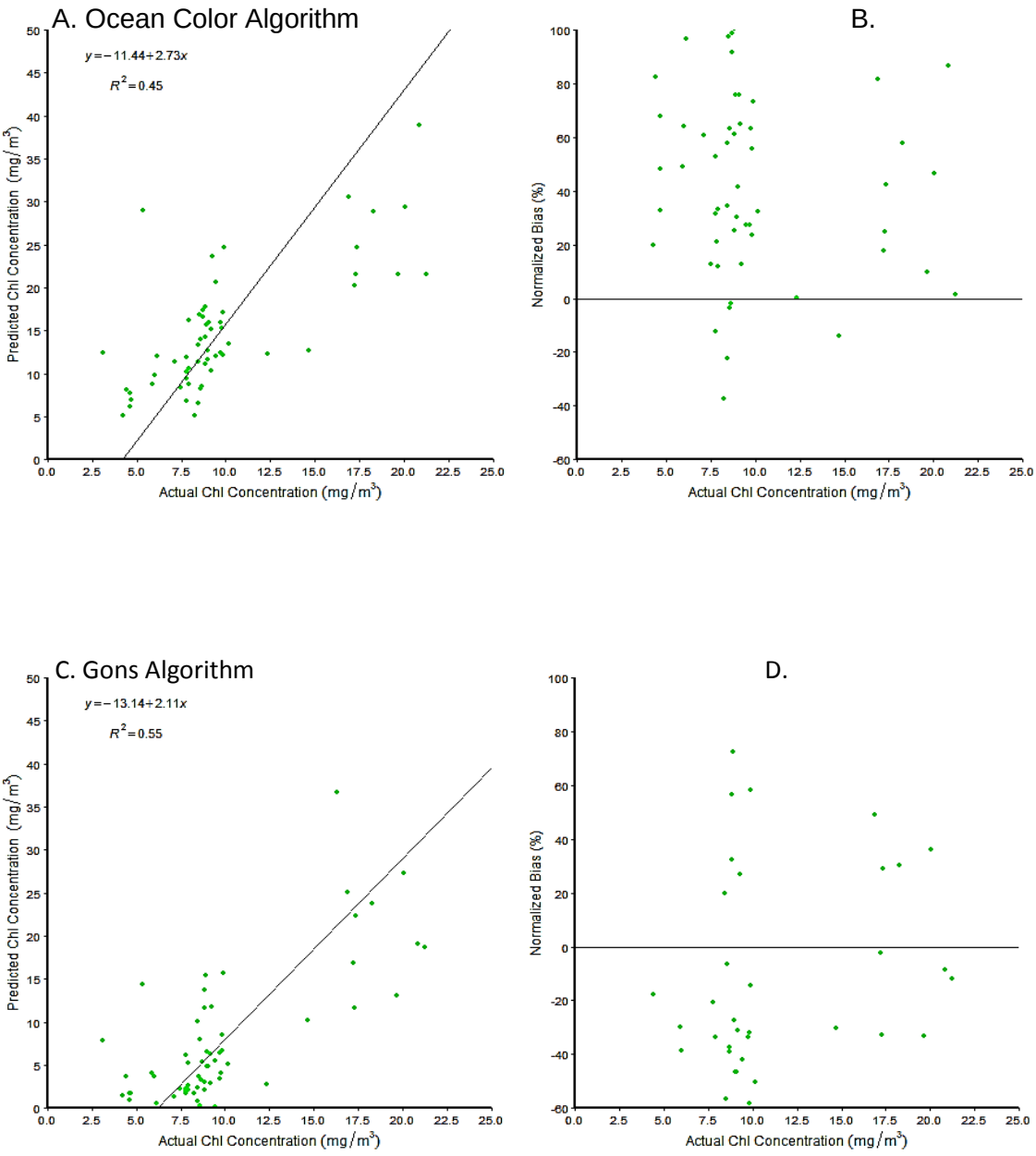
A. Ocean Color Algorithm
y = −11.44+2.73x
R² = 0.45
Predicted Chl Concentration (mg/m³)
Actual Chl Concentration (mg/m³)
B.
Normalized Bias (%)
Actual Chl Concentration (mg/m³)
C. Gons Algorithm
y = −13.14+2.11x
R² = 0.55
Predicted Chl Concentration (mg/m³)
Actual Chl Concentration (mg/m³)
D.
Normalized Bias (%)
Actual Chl Concentration (mg/m³)

E. Ruddick Algorithm

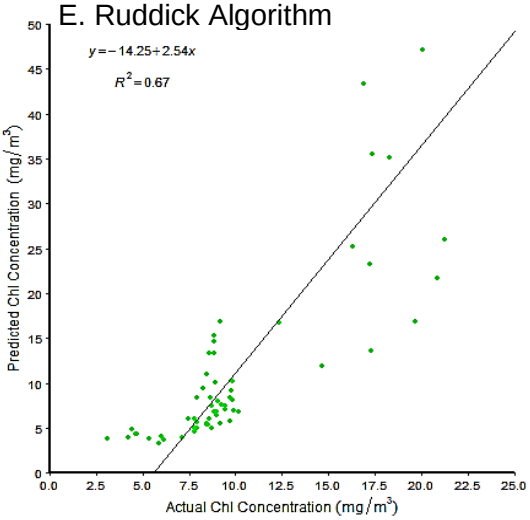

F.

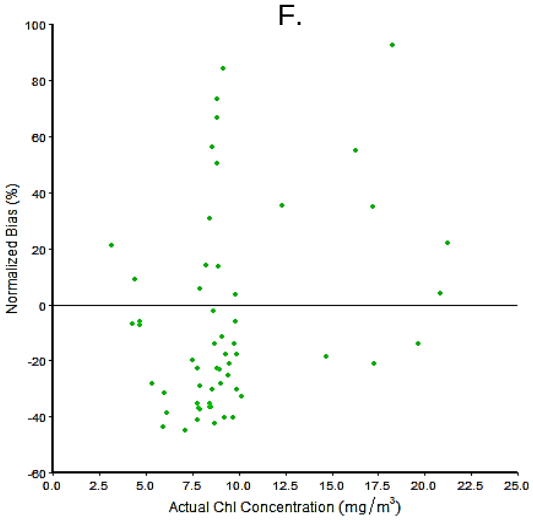

G. Gitelson Algorithm

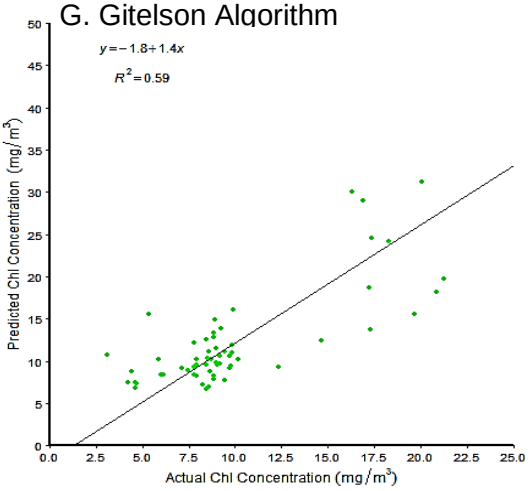

H.

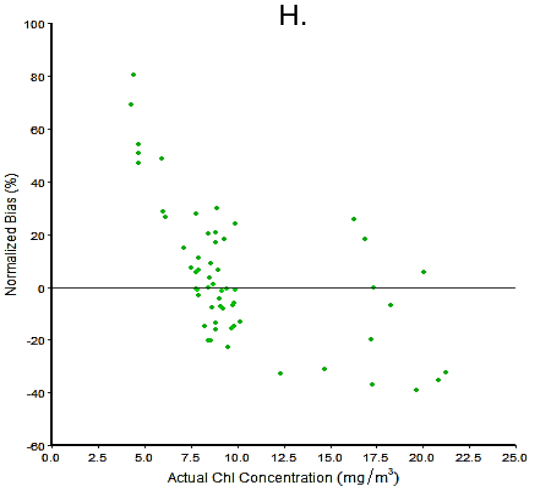

FIG. 4. The left graphs (A,C,E,G) show the results of a type II regression on modelled chlorophyll *a* concentration vs. measured chlorophyll *a* concentration. The graphs on the right (B, D, F, H) show the mean normalized bias for measured chlorophyll. A and B are for the OC4v.4 algorithm. C and D are for the Gons algorithm. E and F are for the Ruddick algorithm, and G and H are for the Gitelson algorithm.

Table 2. Statistical results of the type two regressions run for the four inversion algorithms

Algorithm Name	Y-int (mg/m^3)	Slope	R^2	RMSE (mg/m^3)	MNB (%)	NRMSE (%)	r test p-value
OC4V4	11.44 ± 5.2	2.73 ± 3.8	0.45	8.85	62.6	16.5	.39
Gons	-13.14 ± 8.98	2.11 ± 2.74	0.55	5.72	-27.1	15.6	.92
Ruddick	14.25 ± 10.29	2.54 ± 3.1	0.67	6.56	.802	15.0	.33
Gitelson	-1.80 ± .86	1.40 ± 1.76	0.59	4.20	28.8	17.1	.82

OC4V4:

The Sea-viewing Wide Field-of-View Sensor (SeaWiFS) bio-optical algorithm (OC4v.4) tended to overestimate chlorophyll *a* (chl-a) by an average of 62.6%, with a high amount of random error, 16.5%. The r^2 relationship between chl-a_{pred} and chl-a_{meas} was .45, with a slope of 2.73 ± 3.8 and an RMSE of *chl-a* prediction of 8.85 mg m^{-3}. A similar study conducted by Harding in the Chesapeake found that OC4v.4 tended to overestimate chlorophyll *a* by $\sim 42\%$ (Harding *et al.* 2005).

Gons:

The low mean normalized bias, -27.2% indicates that this algorithm was mostly underestimating chlorophyll *a* levels. However, there was also a high amount of random error, 15.6%. The r^2 relationship between chl-a_{pred} and chl-a_{meas} was .55, higher than the fit of OC4v.4. The slope was 2.73 ± 3.8 and the RMSE of chl-a prediction was 8.85 mg m^{-3}. The scatter around the measured value is most likely due to the varying a*. A* is known to vary based on the composition of phytoplankton species, the compartmentalization of pigment, the intracellular absorption coefficient and the aggregation of phytoplankton (Gons 1999).

Ruddick:

This model had an overall low level of bias, .802%, however it still had high random error, 15.0%. The r^2 relationship between chl-a_{pred} and chl-a_{meas} was .67, higher than the fit of Gons. The slope was 2.54 ± 3.1 and the RMSE of chl-a prediction was 6.56 mg m^{-3}. Ruddick's algorithm exhibited similar inconsistency

as Gons, however it tended to underestimate chlorophyll *a* concentration less so than Gons, it also yielded a lower overall RMSE value.

Gitelson:

The r^2 relationship between chl-a_{pred} and chl-a_{meas} was .59 , lower than that of Ruddick, but higher than the fit of Gons. The slope was 1.40 ± 1.76 and the RMSE of chl-a prediction was 4.20 mg m^{-3}. This algorithm had the lowest overall level of scatter around the regression line (fig. 1G), and the lowest level of RMSE, 4.20 mg m^{-3}.

Summation:

The results of the Pearson coefficient (r) test, suggest that none of the algorithms performed significantly better than the average performance of all of the algorithms. It seemed that OC4v.4 was the worst predictor of chlorophyll *a*. It tended to overestimate the chlorophyll concentration (MNB = 62.6%) in an inconsistent way (NRMSE = 16.5%). Ruddick's algorithm seems to have successfully improved upon the Gon's algorithm: the mean normalized bias improved dramatically (MNB_{Gons} =-27.1%, $MNB_{Ruddick}$=.802%), however both algorithms exhibited high degrees of random error ($RMSE_{Gons}$ =-15.6%, $RMSE_{Ruddick}$=15.0%). The Gitelson algorithm had a slope closest to one, a y intercept closest to zero, and the lowest absolute error (RMSE=4.20 mg/m^{-3}), however it still exhibited high systematic and random errors (MNB=28.8%, NRMSE=17.1%).

Discussion:

In order to best understand my results, I will discuss each algorithm individually. In my discussion, I will evaluate the assumptions made by the modelers and attempt to explain model performance in light of the unique optical properties of the Choptank River. Relative to inland bodies of water, and the open ocean, the Choptank River experiences a high degree of temporal heterogeneity with respect to levels of dissolved nutrients, sediment, and phytoplankton species assemblage and abundance (Kemp *et al.* 2005). Of the algorithms tested, only Gitelson's algorithm was developed and parameterized to the Chesapeake Bay and the Choptank River.

Qualitative Data:

The gradient described in Figure 3 ensured that each of the algorithms was tested in a range of optical conditions. The gradient was most likely caused by the increased rate of sediment loading due to the preponderance of agricultural lands in the northern Choptank River (Darrell 1998).

Quantitative Data:

As stated above, to better understand the performance of each individual algorithm, I will analyze each of the algorithms and attempt to explain their performance.

OC4V4:

The Sea-viewing Wide Field-of-View Sensor (SeaWiFS) bio-optical algorithm (OC4v.4) developed by O'reilly *et al.* (2000) takes a ratio of green light

to blue light. The green wavelength is always set to 555 nm, the blue light is either 443 nm, 490 nm, or 510 nm depending on which wavelength would yield the highest $R_{RS}(\lambda)$ ratio. (eq. 7).

$$R_{max} = \log_{10}(R_{RS}{}_{555}^{443} > R_{RS}{}_{555}^{490} > R_{RS}{}_{555}^{510}) \quad (7)$$

The algorithm then uses R_{max} as a coefficient in a fourth order polynomial (eq. 8).

$$chl\ a = 10^{(.366-3.067R_{max}+1.930R_{max}^2+.649R_{max}^3-1.532R_{\max}^4)} \quad (8)$$

The previous blue/green algorithm used two wavelengths, 490 and 455 nm (O'reilly *et al.* 2000). The OC4V4 iteration proved to substantially increase the model's agreement with lab measurements of chlorophyll *a* in case I waters (O'reilly *et al.* 2000).

The high degree of systematic bias we found (MNB = 62.6%) in this algorithm was not surprising as this algorithm is designed for use in case I waters, where chlorophyll *a* tends to be the dominant reflector of light at 555 nm (O'reilly *et al.* 2000). In case II waters, both chlorophyll *a* and sediment strongly reflect green light. Therefore, the algorithm tended to overestimate the level of chlorophyll in the water, i.e., the algorithm could not distinguish the reflectance attributable to sediment from the reflectance attributable to chlorophyll a (O'reilly *et al.* 2000).

All of the following algorithms were designed specifically for case II waters with the purpose of accurately differentiating the reflectance due to sediment from the reflectance due to chlorophyll *a*.

Gons:

Instead of using the reflectance peak in the green wavelengths, biological oceanographers utilize the reflectance minimum in the red wavelengths (672 nm) in case II waters. Using the definition of RRS as described in Equation 1, Gons wrote the reflectance ratio of 704 nm and 672 nm, *R,* as,

$$R = (a_{672} + b_{672})/(a_{704} + b_{704}) \quad (9)$$

Gons (1999) made the following three assumptions to isolate the concentration of Chlorophyll *a* from equation 9:

1) Water absorption dominates at 672 nm.

2) Water absorption dominates at 704 nm.

3) Total scattering is wavelength independent over these wavebands.

a_{672}^{*} is designed to normalize the absorbance of phytoplankton to the absorbance of chlorophyll (Gons 1999). a_{672}^{*} relates the absorbance of phytoplankton to the absorbance of Chlorophyll *a* according to,

$$a_{phy}/a_{chl} \quad (10)$$

By regressing equation 9 with data collected in a range of estuaries and lakes, Gons (1999) found a_{672}^{*} to be equal to .0175 ± .00003. Gons (1999) used standard absorbance values for water to derive a_{w704} and a_{w672}.

b_b is the sum of the backscattering of particulates in the visible spectrum. This factor is found by multiplying the reflectance at 776 nm by a scaling factor. The scaling factor has not been empirically derived for the Chesapeake Bay, but

most biological oceanographers use a value of .287 for case II waters (Gons 1999).

By making the above assumptions and using the above parameters, the concentration of Chlorophyll *a* can then be described as,

$$chla = \{R * (a_{w704} + b_b) - a_{w672} - b_b\}/a^*_{672} \quad (11)$$

I did not discern a clear pattern of systematic error for this algorithm, although overall the model tended to under-predict the chlorophyll *a* concentration (RMB = -27.1%). Because the Choptank River is subject to a high influx of sediment, it is possible that the scaling factor used for most case II waters was not high enough. It is also possible that the size of sediment in the Choptank River was not constant throughout the study duration, and because the optical properties of sediment depends on their size, b_b may not have been constant across all stations, at all times (Kirk 2011).

Ruddick:

Like Gons' algorithm, Ruddick's algorithm used a ratio of reflectance to remove the effects of sediment backscattering. Ruddick's algorithm finds two wavelengths around 672 nm for which RRS is equivalent (Figure 5). If the following two assumptions are made,

1) The backscattering due to sediment, CDOM, and phytoplankton is constant in these two wavebands, and,

2) The absorbance due to sediment and CDOM is constant in these two wavebands,

Then a ratio of the two RRS terms, will leave only the absorbance of water and the absorbance due to phytoplankton. Then, by taking the known absorbance of water at both wavelengths, the two terms can be subtracted, and the residual absorbance value should be attributable only to chlorophyll. Ultimately chlorophyll *a* concentration, *C* is set to,

$$C = a'_w / a^*_{672} \tag{12}$$

Where,

$$a'_w = a_{w2} - a_{w1} \tag{13}$$

Based on data collected by Ruddick (2001) in a variety of case II waters, a^*_{672} was set to 0.0176.

The following figure explains in detail how the two wavebands (from which a_{w1} and a_{w2} are determined) are selected.

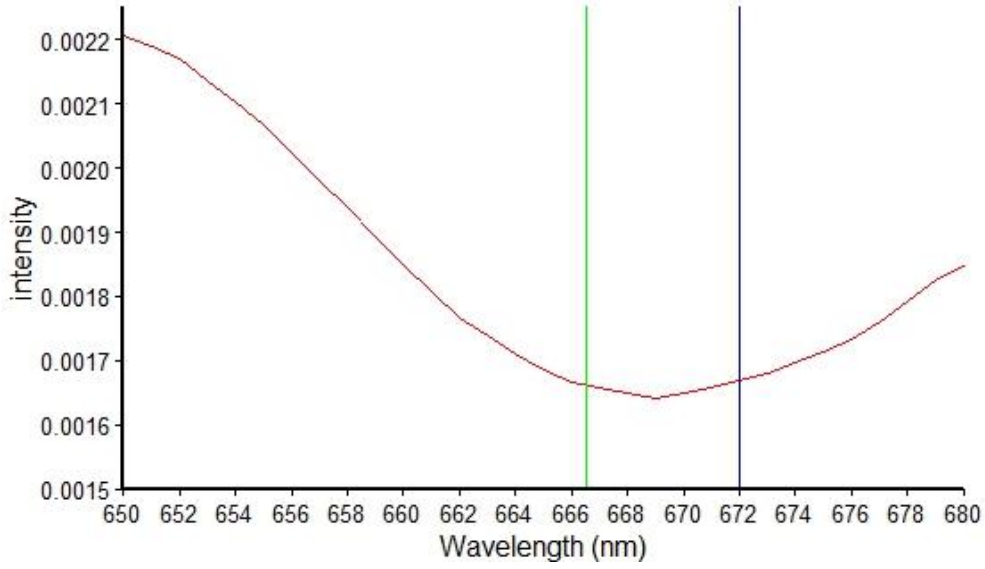

FIG. 5. Explanation of the Ruddick algorithm for an arbitrary reflectance spectrum (Ruddick 2001).

The first waveband is always set to 672 nm (violet line), the second waveband (green line) is the nearest wavelength where the reflectance is within 1% of the first wavelength.

Ruddick's model yielded a low level of systematic error (RMB = .802%). The algorithm did not exhibit a propensity to under or over predict the level of chlorophyll, however the magnitude of error still tended to be very high (Figure 4F).

Ruddick's model assumed that the backscattering and absorption of particulate matter was equivalent in both wavebands selected (Ruddick 2001). Although the backscattering of sediment in these wavebands is most likely close, the absorption due to sediment may well be variable (Kirk 2011, Gitelson 2008).

Gitelson:

Gitelson's algorithm isolates the absorbance of phytoplankton at 665 nm by subtracting the reciprocal reflectance at 665 nm by the reciprocal reflectance at 715 nm.

Because of the following assumptions,

1) Absorbance due to particulate matter and CDOM is constant in these near IR wavebands, and

2) The scattering of particulate matter is constant in the near IR bands,

when the two reflectance values are subtracted, their difference is proportional to the absorbance of Chlorophyll *a* multiplied by the absorbance of water and the scattering by particulate matter. To isolate the absorbance due to

chlorophyll *a,* the difference of the first two wavebands is multiplied by a longer waveband, 750 nm. Because Gitelson (2008) assumed that in this waveband only the absorbance of water and the scattering due to particulate matter was influencing the reflectance value, the resulting product is simply the absorption due to Chlorophyll *a*. After tuning his algorithm in the waters of the Chesapeake Bay, Gitelson (2008) derived his three-band algorithm,

$$chla = 15.811 * 70.712(RRS_{665}^{-1} - RRS_{715}^{-1}) * RRS_{750} \qquad (14)$$

When Gitelson (2008) evaluated his algorithm in the Choptank River, he obtained the following statistics, NRMSE = 21.1%, MNB = 11.1%, and RMSE=3.5 mg m^{-3}. These results are comparable to my own, NRMSE=17.1%, MNB = 28.8% and RMSE = 4.20 mg m^{-3}. Examining graph 1H reveals that there is still a large amount of bias, although compared to all the other algorithms, the magnitude of bias seemed to be the least drastic. Gitelson (2008) found that his algorithm could maintain acceptable levels of accuracy in waters which were characterized by a large degree of variation in the dissolved matter (phytoplankton, sediment, and CDOM), and amongst different taxa of phytoplankton, such as the Chesapeake Bay (Gitelson 2008). My results are generally in line with Gitelson's findings.

Conclusion:

For simple linear regression models, a slope close to one and an intercept close to zero is an indication that the model is accurately predicting *in situ* data (Brewin *et al.*, 2015). MNB and NRMSE should also be close to zero (Brewin *et al.* 2015). My results suggest that an increased understanding of the variation of optically active constituents in the water column is necessary to refine current inversion models. Of the four algorithms tested, Gitelson's three-band algorithm provided the most satisfying closure. In the future, an algorithm like Gitelson's will be refined using precisely measured inherent optical properties of the Chesapeake Bay.

Although some amount of *in situ* error was statistically accounted for in the type II regression, in future studies it would be wise to include more trials of in situ data to create an index of *in situ* error. Furthermore, because there is uncertainty in the *in situ* data, it may not be wise to compare the performance of the four algorithms to the average performance of the algorithms using the z test. Additional sources of lab measured chlorophyll *a* error are discussed below.

Error in my lab measurements of Chlorophyll *a* may have impacted the accuracy of the optical inversion algorithms. The flourometer fires blue light at a water sample and then determines the chlorophyll *a* concentration by relating the emitted red light to a standard curve determined for pure chlorophyll a. However, because there are other light capturing pigments utilized by phytoplankton, the fluorometer was most likely over-predicting chlorophyll *a* levels (Holm-Hansen 1965). In 1965, Holm-Hansen found that photosynthetic pigments are not the only biological materials that fluoresce red light upon the excitation of blue light.

Various porphyrins and metalloporphyrins also fluoresce in the measured waveband (Holm-Hansen 1965). Other factors that influence the accuracy of fluorometric analysis of chlorophyll *a* include the reabsorption of emitted red light by other pigments, the quenching of the emitted red light by beta carotene, and the oxidization of exposed chlorophyll molecules which diminishes their fluorescence (Holm-Hansen 1965).

Because typical sampling studies focus solely on the identification of Chlorophyll *a*, there is little information on the relative abundances of other chlorophyll molecules in the Chesapeake Bay. New technologies such as High Pressure Liquid Chromatography (HPLC) will allow precise pigment measurements. In the 1980's HPLC emerged as the definitive method of measuring all aquatic pigments, surpassing the accuracy of both spectrometric and fluorescent analyses (Bidigare *et al.* 1985). HPLC not only measures Chlorophyll *a* but all light capturing pigments. HPLC is the most technologically advanced method of chromatography currently used in pharmaceutical, agrochemical and other involatile substance analysis (Lough 1995). A pulse-free pump is used to inject the analyte into a column containing 5 μm porous, spherical particles with a narrow size distribution. The resulting separation of particles can then be resolved by measuring the UV absorbance of the column (Lough 1995). HPLC analyses are expensive and time consuming, and therefore not used in this study.

Chlorophyll *a* is undoubtedly the most common pigment molecule in the open ocean, however in turbid environments with unique light fields, selection may favor the preponderance of phytoplankton with different compositions of

light-capturing pigments (Stomp *et al.* 2007). Because the presence of particulate matter and CDOM attenuates the light field as a function of their volume, shape, and chemical composition, the wavebands of light reaching phytoplankton are substantially different between case II waters and case I waters (Mobley 1999). Because light energy is a limiting resource for phytoplankton, natural selection would favor the phytoplankton species that most efficiently capture the available bands of light energy (Stomp *et al.* 2007). Phytoplankton in the Chesapeake Bay would then be expected to exhibit a variety of light capturing molecules uniquely adapted to the available light field in their environment. Using HPLC, studies could attempt to verify this hypothesis as well as better quantify the pigments utilized by phytoplankton in the Chesapeake Bay and all case II waters. New technology will also provide for more accurate inversion algorithm development. A discussion of the current drawbacks in case II inversion algorithms is discussed below.

Most case II inversion algorithms seek to exploit the relatively narrow band at which chlorophyll *a* preferentially absorbs light, namely 672 nm (Kirk 2011). This strategy is currently the most prevalent in the literature, but there are some simplifications made by modelers (Ruddick 2001, Gons 1999, O'reilly *et al.* 2000, Gitelson 2008). Most models assume that the only pigment phytoplankton are using is chlorophyll *a.* However other pigments, especially chlorophylls *b* and *c*, have overlapping absorption spectrums in the wavebands utilized by the inversion algorithms (Stomp *et al.* 2007). Therefore, the optical properties of these pigments in the water column would have decreased the reflectance

minimum at 672 nm, and therefore would have caused inaccurate chlorophyll *a* retrievals. The following two figures aim to emphasize this point.

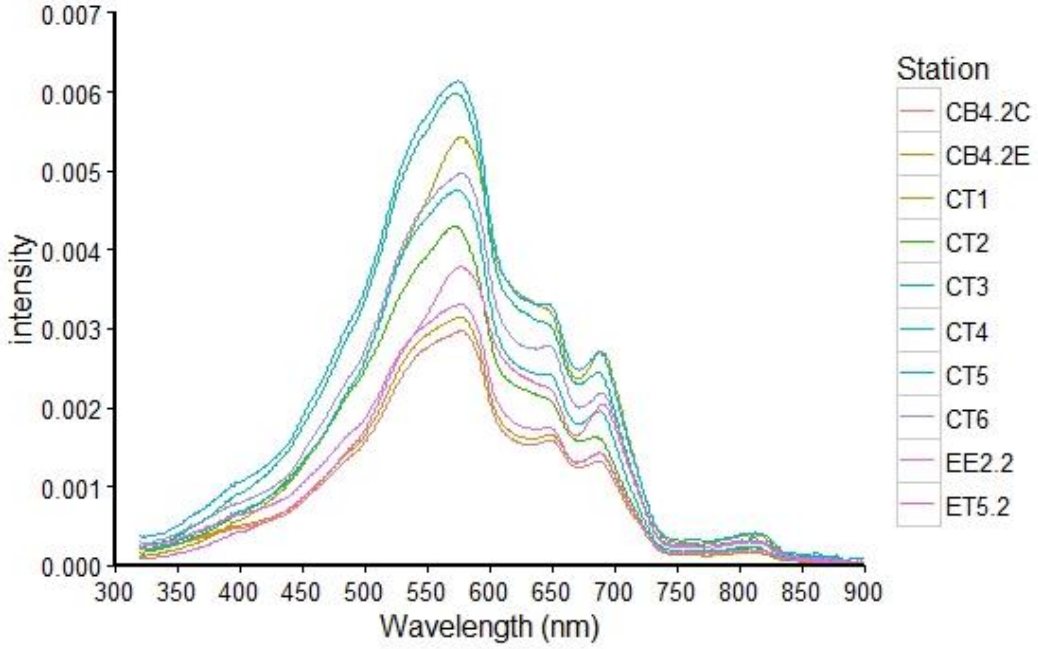

FIG 6. Entire transect light spectra for 07/06/2016 along the mainstem Choptank River transect.

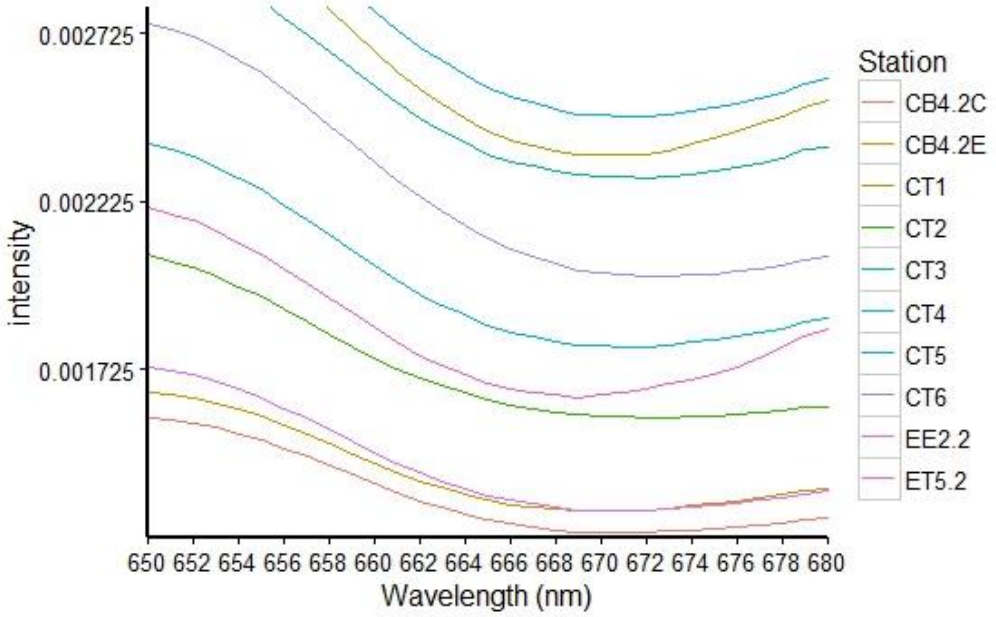

FIG 7. The 07/06/2016 mainstem Choptank River transect zoomed into the reflectance minima around 672 nm.

As figures 5 and 6 make clear, the local minima occur before 672 nm, which would not happen if chlorophyll *a* was the only particle actively absorbing in these wavebands in the water.

Inversion algorithms also assume that there is no absorption by dissolved organic matter or detritus in the wavelengths near 672 nm. More advanced algorithms, such as Gitelson's, assume that the absorbance by other particles is constant within the range of 550-770 nm, and thus corrections can be made wholly using reflectance information (Gitelson 2008). Far more desirable than inferring inherent optical properties from the reflectance information would be to directly measure the absorbance and backscattering properties of components in the water column (Tzortziou 2011). When inherent optical properties can be empirically measured using sophisticated profilers, these exact model parameters can be incorporated into existing algorithms and be used to create site-specific algorithms with a high degree of accuracy (Tzortziou 2011). Manufacturers such as WET labs (Philomath, Oregon) recently began selling optical profilers which can measure inherent optical properties of CDOM, sediment, and phytoplankton.

Greg Silsbe is currently using one of these profilers on the Choptank River to directly sample the optical properties of phytoplankton, sediment, and CDOM at discrete depths throughout the photic zone (Silsbe, pers. comm.). Using this spectral information, modelers will no longer need to assume that chlorophyll *a* is the only pertinent absorbing molecule used by phytoplankton, instead the absorptive properties of phytoplankton can be measured directly (Silsbe, pers. comm.). Because the absorptive properties of phytoplankton depend on their

size, and pigment concentration, the added spectral information may be used in the future to identify functional groups of phytoplankton. For example, a high concentration of very small reflective, phytoplankton typically indicates a coccolithophore bloom (Nair *et al.* 2008). Phytoplankton species abundance has been found to have implications on the species abundance of heterotrophs such as fish and crab (Ulanowicz 1988). In the Chesapeake Bay, menhaden populations were correlated to dinoflagellate populations (Ulanowicz 1988). A more precise understanding of the exact optical properties of phytoplankton in the Chesapeake Bay will allow for a greater understanding of the entire estuarine food web.

Besides using the absorbance maximum of chlorophyll, *a,* some algorithms attempt to use the fluorescence peak of chl a in the 700 nm waveband. Although my study did not test these algorithms, a discussion of their usage may prove salient as algorithms will continue to be developed and refined in the future. The strong scattering peak by particulate matter in the fluoresced wavebands greatly complicates isolating the phytoplankton fluorescent signal (Hliang 2007). Based on his 2007 study in the Chesapeake Bay, Hliang found that fluorescence reflectance could be incorporated into existing algorithms to yield increasingly accurate chlorophyll *a* predictions. However, their results were obfuscated by a lack of understanding of specific chlorophyll absorption spectra, and complex illumination schemes. Consequently, more detailed field studies are necessary before a satisfactory algorithm that utilizes fluorescence information is usable (Hliang 2007).

Remote sensors are currently faced with the challenge of accurately evaluating relevant water quality metrics in dynamic marine environments subject to large amounts of seasonal, and decadal change (Ruddick 2000). Thus far, significant progress has been made in the case I waters of the open ocean, and satisfying carbon cycling budgets can be extrapolated from MODIS gathered data (Silsbe 2016). Currently, oceanographers are seeking to seamlessly retrieve accurate water quality parameters in both case I and case II waters. A better understanding of the carbon cycle in extremely productive ecosystems such as the Chesapeake Bay must begin with accurate quantification of phytoplankton populations.

The use of hyperspectral radiometers, which have broader spectral ranges and higher resolutions than multispectral radiometers, represents an important advancement in biological oceanography. The launch of the PACE satellite in 2020 will mark the first time in which high spectral resolution data will be available for coastal and estuarine waters. The greater spectral detail will allow modelers to use reflectance information from more wavelengths to better differentiate the reflectance of phytoplankton from the reflectance of sediment and CDOM. More accurate phytoplankton population information will allow for more accurate NPP estimates and increased understanding of phytoplankton population. These biological processes have implications on wild fish catches, upon which 13% of the world relies for protein, and on the warming of our planet (FAO 2016, Riebesell 2007).

References

Anderson, T. R., W. C. Gentleman, and B. Sinha. 2010. Influence of grazing formulations on the emergent properties of a complex ecosystem model in a global ocean general circulation model. Progress in Oceanography 87:201–13.

Bacher, C., P. Duarte, J. G. Ferreira, M. Heral, and O. Raillard. 1998. Assessment and comparison of the Marennes–Oleron Bay (France) and Carlingford Lough (Ireland) carrying capacity with ecosystem models. Aquatic Ecology 31:379–394.

Baird, D. and R.E. Ulanowicz, 1989. The seasonal dynamics of the Chesapeake Bay ecosystem. Ecological monographs, 59(4), pp.329–364.

Behrenfeld, M. J. 2010. Abandoning Sverdrup's Critical Depth Hypothesis on phytoplankton blooms. Ecology 91:977–89.

Behrenfeld, M. J., S.C. Doney, I. Lima, E.S. Boss, and D.A. Siegel. 2013. Physical-ecological interactions of the subarctic Atlantic annual plankton bloom. Global Biogeochemical Cycles. 27:526–40.

Bidigare, R., M. Kennicutt, and J. Brooks. 1985. Rapid determination of chlorophylls and their degradation products by high-performance liquid chromatography. Limnology and Oceanography 30:432–435.

Bidigare, R. R., M. E. Ondrusek, J. H. Morrow, and D. A. Kiefer. 1990, September. In-vivo absorption properties of algal pigments. Pages 290-302 *in Orlando'90, 16–20 April*. *International Society for Optics and Photonics*. Orlando, Florida.

Boicourt, W. C. 1992. Influences of circulation processes on dissolved oxygen in the Chesapeake Bay. Pages 7–59 *in* D.E. Smith M. Leffler, and G. Mackiernan, editors, Oxygen dynamics in the Chesapeake Bay: a synthesis of recent research. Academic. Annapolis, Maryland.

Bopp L, et al. 2001. Potential impact of climate change on marine export production. Global Biogeochem Cycles 15:81–100.

Borges, A. V. 2005. Do we have enough pieces of the jigsaw to integrate CO2 fluxes in the coastal ocean? Estuaries. 28:3–27.

Boss, E., and M. J. Behrenfeld. 2010. *In situ* evaluation of the initiation of the North Atlantic phytoplankton bloom. Geophysical Research Letters 37:L18603.

Boyce, D. G., M. R. Lewis, and B. Worm. 2010. Global phytoplankton decline over the past century. Nature 466:591–596.

Boyd, P. W., A. J. Watson, C. S. Law, E. R. Abraham, T. Trull, et al. 2000. A mesoscale phytoplankton bloom in the polar Southern Ocean stimulated by iron fertilization. Nature 407:695–702.

Boyd, P. W., C. S. Law, C. S. Wong, Y. Nojiri, and A. Tsuda. 2004. The decline and fate of an iron-induced subarctic phytoplankton bloom. Nature 428:549–53.

Bukata, R. P., J. H. Jerome, K. Y. Kondratyev, and D. V. Pozdnyakov. 1995. Optical properties and remote sensing of inland and coastal waters. First edition. CRC Press, Inc., Boca Raton, Florida, USA.

Calbet A., and M. R. Landry. 1999. Mesozooplankton influences on the microbial food web: direct and indirect trophic interactions in the oligotrophic open ocean. Limnology and Oceanography. 44:1370–80.

Canfield, D. E. 2005. The early history of atmospheric oxygen: homage to Robert M. Garrels. Annu. Rev. Earth Planet. Sci. 33:1–36.

Cebrian, J. 1999. Patterns in the fate of production in plant communities. American Naturalist 154:449–468, doi:10.1086/303244.

Chen, Z., C. Hu, and F. Muller-Karger. 2007. Monitoring turbidity in Tampa Bay using MODIS/Aqua 250-m imagery. Remote Sensing of Environment 109:207–220.

Cloern, J. E. 1987. Turbidity as a control on phytoplankton biomass and productivity in estuaries. Cont. Shelf Res. 7:1367–1381.

Cloern, J. E., S. Q. Foster, and A.E. Kleckner. 2014. Phytoplankton primary production in the world's estuarine-coastal ecosystems. Biogeosciences 11:2477–2501.

Coale, K. H., K. S. Johnson, S. E. Fitzwater, R. M. Gordon, S. Tanner, et al. 1996. A massive phytoplankton bloom induced by an ecosystem-scale iron fertilization experiment in the equatorial Pacific Ocean. Nature 383:495– 501.

Costanza, R., R. d'Arge, R. deGroot, S. Farber, M. Grasso, B. Hannon, K. Limburg, S. Naeem, R. V. Oneill, J. Paruelo, R. G. Raskin, P. Sutton, and M. vandenBelt. 1997. The value of the world's ecosystem services and natural capital. Nature 387:253–260.

Curry, R., and C. Mauritzen. 2005. Dilution of the northern North Atlantic Ocean in recent decades. Science 308:1772–1774.

Darrell, L. C., B. F. Majedi, J. S. Lizarraga, and J. D. Blomquist. 1999. Nutrient and suspended-sediment concentrations, trends, loads, and yields from the nontidal part of the Susquehanna, Potomac, Patuxent, and Choptank rivers, 1985–96. US Department of the Interior, US Geological Survey.

de Baar, H. J. W., P. W. Boyd, K. H. Coale, M. R. Landry, A. Tsuda, et al. 2005. Synthesis of iron fertilization experiments: from the Iron Age in the Age of Enlightenment. Journal of Geophysical Research 110:C09S16.

Dickey, T. D., G. W. Kattawar, and K. J. Voss. 2011. Shedding new light on light in the ocean. Physics Today 64:44–49.

Duan, S., S. S. Kaushal, P. M. Groffman, L. E. Band, and K. T. Belt, K.T. 2012. Phosphorus export across an urban to rural gradient in the Chesapeake Bay watershed. Journal of Geophysical Research: Biogeosciences. *117*(G1).

Duarte, C. M. and J. Cebrian. 1996. The fate of marine autotrophic production, Limnology and Oceanography 41:1758–1766.

Falkowski, P., R. Scholes, E. Boyle, J. Canadell, D. Canfield, J. Elser, N. Gruber, K. Hibbard, P. Högberg, and S. Linder. 2000. The global carbon cycle: a test of our knowledge of earth as a system. Science 290:291–296.

FAO. 2016. Contributing to food security and nutrition for all. The State of World Fisheries and Aquaculture 2016. Rome.

Flores, F. G., and A. Herrero. 2008. The cyanobacteria: molecular biology, genomics, and evolution. Horizon Scientific Press.

Gitelson, A. A., J. F. Schalles, and C. M. Hladik. 2007. Remote chlorophyll-a retrieval in turbid, productive estuaries: Chesapeake Bay case study. Remote Sensing of Environment 109:464–472.

Gons, H. J., 1999. Optical teledetection of chlorophyll a in turbid inland waters. Environmental Science and Technology. 33:1127–1132.

Gregory, J., K. Dixon, R. Stouffer, A. Weaver, E. Driesschaert, M. Eby, T. Fichefet, H. Hasumi, A. Hu, and J. Jungclaus. 2005. A model intercomparison of changes in the Atlantic thermohaline circulation in response to increasing atmospheric CO_2 concentration. Geophysical Research Letters 32.

Hagy, J. D., W. R. Boynton, C. W. Keefe, and K. V. Wood. 2004. Hypoxia in Chesapeake Bay, 1950–2001: long-term changes in relation to nutrient loading and river flow. Estuaries. 27:634–658.

Hedges, J. I. 1992. Global biogeochemical cycles: progress and problems. Marine chemistry 39:67–93.

Holligan, P., and W. Reiners. 1992. Predicting the responses of the coastal zone to global change. Advances in Ecological Research 22:211–255.

Holm-Hansen, O., C. J. Lorenzen, R. W. Holmes, and J. D. Strickland. 1965. Fluorometric determination of chlorophyll. *Journal du Conseil*, *30*(1), pp.3–15.

Jaworski, N. 1990. Retrospective of the water quality issues of the upper Potomac estuary. Aquatic Sciences 3:11–40.

Kemp, W. M., W. R. Boynton, J. E. Adolf, D. F. Boesch, W. C. Boicourt, G. Brush, J. C. Cornwell, T. R. Fisher, P. M. Glibert, J. D. Hagy, L. W. Harding Jr., E. D. Houde, D. G. Kimmel, W. D. Miller, R. I. E. Newell, M. R. Roman, E. M. Smith, and J. C. Stevenson. 2005. Eutrophication of Chesapeake Bay: historical trends and ecological interactions, Marine Ecology Progress Series 303:1–29.

Kemp, W., E. Smith, M. Marvin-DiPasquale, and W. Boynton. 1997. Organic carbon balance and net ecosystem metabolism in Chesapeake Bay. Marine Ecology Progress Series 150:229–248.

Kirk, J. 2011. Light and photosynthesis in aquatic ecosystems, 3rd ed. Cambridge University Press.

Landry M. R., J. Constantinou, M. Latasa, S. L. Brown, R. R. Bidigare, and M. E. Ondrusek. 2000. Biological response to iron fertilization in the eastern equatorial Pacific (IronEx II). III. Dynamics of phytoplankton growth and microzooplankton grazing. Marine Ecology Progress Series 201:57–72.

Lee, Z. P., N. Pahlevan, Y. H. Ahn, S. Greb, and D. O'Donnell. 2013. Robust approach to directly measure water-leaving radiance in the field. Applied Optics 52:1693 –1701.

Levitus, S., J. I. Antonov, T. P. Boyer, and C. Stephens. 2000. Warming of the world ocean. Science 287:2225–2229.

Longhurst, A., S. Sathyendranath, T. Platt, and C. Caverhill. 1995. An estimate of global primary production in the ocean from satellite radiometer data. Journal of plankton Research 17:1245–1271.

Lough, W. J., and I. W. Wainer. 1995. High performance liquid chromatography: fundamental principles and practice. CRC Press.

MacIntyre, H. L., E. Lawrenz. and T. L. Richardson. 2010. Taxonomic discrimination of phytoplankton by spectral fluorescence. Pages 129–169 *in* D.J. et al., editors. Chlorophyll a fluorescence in aquatic sciences: methods and applications. Springer Science, Dordrecht, The Netherlands.

Magnuson, A., L. W. Harding, M. E. Mallonee, and J. E. Adolf. 2004. Bio-optical model for Chesapeake Bay and the Middle Atlantic Bight. 2004. Estuarine, Coastal and Shelf Science. 61:403–424.

Mariani P., K. H. Andersen, A. W. Visser, A.D. Barton, and T. Kiørboe. 2013. Control of plankton seasonal succession by adaptive grazing. Limnology and Oceanography 58:173–84.

Marshall, H. G., L. Burchardt, and R. Lacouture, 2005. A review of phytoplankton composition within Chesapeake Bay and its tidal estuaries. Journal of Plankton Research, 27(11), pp.1083–1102.

Martin, S. 2014. An introduction to ocean remote sensing, 2nd ed. Cambridge University Press.

McGuire, A. D., J. M. Melillo, D. W. Kicklighter, Y. Pan, X. Xiao, J. Helfrich, B. Moore, C. J. Vorosmarty, and A. L. Schloss. 1997. Equilibrium responses of global net primary production and carbon storage to doubled atmospheric carbon dioxide: Sensitivity to changes in vegetation nitrogen concentration. Global biogeochemical cycles 11:173–189.

Mcleod, E., G. L. Chmura, S. Bouillon, R. Salm, M. Björk, C. M. Duarte, C. E. Lovelock, W. H. Schlesinger, and B. R. Silliman. 2011. A blueprint for blue carbon: toward an improved understanding of the role of vegetated coastal habitats in sequestering CO2. Frontiers in Ecology and the Environment 9:552–560.

Meyer-Arendt, J. R. 1972. Introduction to Classical and Modern Optics. Fourth edition. Prentice-Hall Inc., Englewood Cliffs, New Jersey, USA.

Mobley, C. D., 1999. Estimation of the remote-sensing reflectance from above-surface measurements. Applied Optics 38(36), 7442–7455.

Morel, A. and B. Gentili, 1991. Diffuse reflectance of oceanic waters: its dependence on sun angle as influenced by molecular scattering contribution. Applied Optics 30(30), 4427–4438.

Morel, A., and L. Prieur. 1977. Analysis of variations in ocean color. Limnology and Oceanography 22:709–722.

Moreno-Madriñán, M. J. and A. M. Fischer. 2013. Performance of the MODIS FLH algorithm in estuarine waters: a multi-year (2003–2010) analysis from Tampa Bay, Florida (USA), Int. J. Remote Sens., 34:6467–6483.

Nair, A., S. Sathyendranath, T. Platt, J. Morales, V. Stuart, M.-H. Forget, E. Devred, and H. Bouman. 2008. Remote sensing of phytoplankton functional types. Remote Sensing of Environment 112:3366–3375.

Nixon, S. W. 1982. Quantifying the relationship between nitrogen input and the productivity of marine ecosystems. Proceedings of the Advanced Marine Technology Conference. 5:57–83.

Nixon, S. W. 1988. Physical energy inputs and the comparative ecology of lake and marine ecosystems. Limnology and Oceanography 33:1005–1025.

O'Reilly, J. E., S. Maritorena, D. A. Siegel, M. C. O'Brien, D. Toole, B. G. Mitchell, M. Kahru, F. P. Chavez, P. Strutton, and G. F. Cota. 2000. Ocean color chlorophyll a algorithms for SeaWiFS, OC2, and OC4: Version 4. SeaWiFS postlaunch calibration and validation analyses, Part 3:9–23.

Pegau, W. S., D. Gray, and J. R. V. Zaneveld. 1997. Absorption and attenuation of visible and near-infrared light in water: dependence on temperature and salinity. Applied optics. 36:6035–6046.

Plattner, G. K., F. Joos, T. Stocker, and O. Marchal. 2001. Feedback mechanisms and sensitivities of ocean carbon uptake under global warming. Tellus B 53:564–592.

Pomeroy, L. R. 1974. The ocean's food web, a changing paradigm. Bioscience 24:499–504.

Pritchard D. W. 1967. Observations of circulation in coastal plain estuaries, p. 37–44. In G. H. Lauff [ed.], Estuaries. Academic.

Pritchard, D. W. 1956. The dynamic structure of a coastal plain estuary. Journal of Marine Research 15:33–42.

Prowe, A. E. F., M. Pahlow, S. Dutkiewicz, M. Follows, and A. Oschlies. 2012. Top-down control of marine phytoplankton diversity in a global ecosystem model. Progress in Oceanography 101:1–13.

Riebesell U., D. A. Wolf-Gladrow, V. Smetacek. 1993. Carbon dioxide limitation of marine phytoplankton growth rates. Nature 361:249 –251.

Riebesell, U., A. Körtzinger, and A. Oschlies. 2009. Sensitivities of marine carbon fluxes to ocean change. Proceedings of the National Academy of Sciences 106:20602–20609.

Riebesell, U., G. Kai, R. Schulz, G. Bellerby, M. Botros, P. Fritsche, M. Meyerhöfer, C. Neill et al. 2007. "Enhanced biological carbon consumption in a high CO2 ocean." Nature 407:545–548.

Roesler, C. S., M. J. Perry, and K. L. Carder. 1989. Modeling in situ phytoplankton absorption from total absorption spectra in productive inland marine waters. Limnology and Oceanography 34:1510–1523.

Ruddick, K. G., H. J. Gons, Rijkeboer, and G. Tilstone. 2001. Optical remote sensing of chlorophyll *a* in case 2 waters by use of an adaptive two-band algorithm with optimal error properties. Applied Optics. 40:3575–35835.

Sarmiento, J. L., and C. Le Quere. 1996. Oceanic carbon dioxide uptake in a

model of century-scale global warming. Science 274:1346.

Schlesinger, W. H. 1991. Biogeochemistry: An analysis of global change. Academic.

Sellner, K. G., R. V. Lacouture, and C. R. Parrish. 1988. Effects of increasing salinity on a cyanobacteria bloom in the Potomac River estuary. Journal of Plankton Research 10:49–61.

Siegenthaler, U., and J. Sarmiento. 1993. Atmospheric carbon dioxide and the ocean. Nature 365:119–125.

Simis, S. G. and J. Olsson. 2013. Unattended processing of shipborne hyperspectral reflectance measurements. Remote Sensing of Environment. 135:202–212.

Smith, S., and J. Hollibaugh. 1993. Coastal metabolism and the oceanic organic carbon balance. Reviews of Geophysics 31:75–89.

Sobczak, W. V., J. E. Cloern, A. D. Jassby, B. E. Cole, T. S. Schraga, and A. Arnsberg. 2005. Detritus fuels ecosystem metabolism but not metazoan food webs in San Francisco estuary's freshwater Delta, Estuaries. 28:124–137.

Son, S., and M. Wang. 2012. Water properties in Chesapeake Bay from MODIS-Aqua measurements. Remote Sensing of Environment. 123:163–174.

Stomp, M. J. Huisman, L. J. Stal, and H. C. Matthijs. 2007. Colorful niches of phototrophic microorganisms shaped by vibrations of the water molecule. The ISME journal 1:271–282.

Sullivan, J. M., and M. S. Twardowski. 2009. Angular shape of the oceanic particulate volume scattering function in the backward direction. Applied Optics 48:6811–6819.

Sullivan, J. M., J. R. Zanveld, C. M. Moore, A. H. Barnard, P. L. Donaghay, and B. Rhoades. 2006. Hyperspectral temperature and salt dependencies of absorption by water and heavy water in the 400–750 nm spectral range. Applied Optics 45:5294–5309.

Sutton, A. J., T. R. Fisher, and A. B. Gustafson. 2010. Effects of restored stream buffers on water quality in non-tidal streams in the Choptank River basin. Water, Air, and Soil Pollution, 208(1–4), pp.101–118.

Sutton, R. T., and D. L. Hodson. 2005. Atlantic Ocean forcing of North American and European summer climate. Science 309:115–118.

Sverdrup, H. U., M. W. Johnson, and R.H. Fleming. 1942. The oceans. Prentice-Hall.

Tassan, S., and G. M. Ferrari. 1995. An alternative to absorption measurements of aquatic particles retained on filters. Limnology and Oceanography 40:1358–1368.

Toggweiler, J., R. Murnane, S. Carson, A. Gnanadesikan, and J. Sarmiento. 2003. Representation of the carbon cycle in box models and GCMs, 2, Organic pump. Global biogeochemical cycles 17.

Tsuda A, S. Takeda, H. Saito, J. Nishioka,Y. Nojiri, et al. 2003. A mesoscale iron enrichment in the western subarctic Pacific induces a large centric diatom bloom. Science 300:958–61.

Twardowski, M. S., J. M. Sullivan, P. L. Donaghay, and J. R. V. Zaneveld. 1999. Microscale quantification of the absorption by dissolved and particulate material in coastal waters with an ac-9. Journal of Atmospheric Oceanic Technology 16:691–707.

Verity P. G., V. Smetacek, T. J. Smayda. 2002. Status, trends and the future of the marine pelagic ecosystem. Environment Conservation 29:207–37.

Verity, P.G., 1988. The trophic structure of pelagic communities: hypotheses and problems. Understanding the estuary: advances in Chesapeake Bay research. Chesapeake Research Consortium Publication. *129*, pp.49–54.

Vitousek, P. M., P. R. Ehrlich, A. H. Ehrlich, and P. A. Matson. 1986. Human appropriation of the products of photosynthesis. Bioscience 36:368–373.

Volk, T., and M. I. Hoffert. 1985. Ocean carbon pumps: Analysis of relative strengths and efficiencies in ocean-driven atmospheric CO2 changes. The Carbon Cycle and Atmospheric CO: Natural Variations Archean to Present:99–110.

Zhang, X. D., L. B. Hu, M. S. Twardowski, and J. M. Sullivan. 2009. Scattering by solutions of major sea salts. Optics Express. 17:19580–19585.

Zimmerman, A. R., and E. A. Canuel. 2002. Sediment geochemical records of eutrophication in the mesohaline Chesapeake Bay. Limnology and Oceanography 47:1084–1093.